Lack of *GAS2L2* Causes PCD by Impairing Cilia Orientation and Mucociliary Clearance

Ximena M. Bustamante-Marin,[1] Wei-Ning Yin,[1] Patrick R. Sears,[1] Michael E. Werner,[2] Eva J. Brotslaw,[3] Brian J. Mitchell,[3] Corey M. Jania,[4] Kirby L. Zeman,[5] Troy D. Rogers,[1] Laura E. Herring,[6] Luc Refabért,[7] Lucie Thomas,[8] Serge Amselem,[8] Estelle Escudier,[8] Marie Legendre,[8] Barbara R. Grubb,[1] Michael R. Knowles,[1] Maimoona A. Zariwala,[9,10,*] and Lawrence E. Ostrowski[1,10,*]

Primary ciliary dyskinesia (PCD) is a genetic disorder in which impaired ciliary function leads to chronic airway disease. Exome sequencing of a PCD subject identified an apparent homozygous frameshift variant, c.887_890delTAAG (p.Val296Glyfs*13), in exon 5; this frameshift introduces a stop codon in amino acid 308 of the growth arrest-specific protein 2-like 2 (GAS2L2). Further genetic screening of unrelated PCD subjects identified a second proband with a compound heterozygous variant carrying the identical frameshift variant and a large deletion (c.867_*343+1207del; p.?) starting in exon 5. Both individuals had clinical features of PCD but normal ciliary axoneme structure. In this research, using human nasal cells, mouse models, and *X.laevis* embryos, we show that GAS2L2 is abundant at the apical surface of ciliated cells, where it localizes with basal bodies, basal feet, rootlets, and actin filaments. Cultured *GAS2L2*-deficient nasal epithelial cells from one of the affected individuals showed defects in ciliary orientation and had an asynchronous and hyperkinetic (*GAS2L2*-deficient = 19.8 Hz versus control = 15.8 Hz) ciliary-beat pattern. These results were recapitulated in *Gas2l2*$^{-/-}$ mouse tracheal epithelial cell (mTEC) cultures and in *X. laevis* embryos treated with *Gas2l2* morpholinos. In mice, the absence of *Gas2l2* caused neonatal death, and the conditional deletion of *Gas2l2* impaired mucociliary clearance (MCC) and led to mucus accumulation. These results show that a pathogenic variant in *GAS2L2* causes a genetic defect in ciliary orientation and impairs MCC and results in PCD.

Introduction

Primary ciliary dyskinesia (PCD) is a rare genetic disorder (MIM: 244400) in which dysfunction of motile cilia[1] results in defective mucociliary clearance (MCC) and chronic airway disease. The clinical features of PCD include neonatal respiratory distress, bronchiectasis, chronic rhinosinusitis, low nasal nitric oxide (nNO) production, male infertility, and a spectrum of laterality defects.[1,2] Genetic variants in >40 genes have been identified in individuals with PCD,[3–12] and ultrastructural cilia defects are observed in ~70% of the cases;[3] however, in many other cases of PCD, the genetic lesions and ciliary defect are still unknown.

The coordinated ciliary beat, with a specific frequency and waveform, directs fluid and foreign materials toward the mouth to be swallowed or expectorated.[13] This coordination results from proper orientation and stabilization of cilia along the tissue axis.[14,15] Stabilization of basal bodies at the surface of ciliated cells provides the foundation for ciliary axoneme extension and the directionality of the ciliary beat.[16] The direction of the ciliary beat is evidenced by the alignment of the basal-body basal foot[16] or basal-body rootlet[17] within individual cells. Mouse models with disrupted rootlets[18] or basal feet[19] suggest that the stabilization of basal bodies is essential for long-term maintenance of ciliary function. In PCD, the ciliary beat and waveform vary from absent to a range of uncoordinated motions,[20,21] impairing MCC and leading to the chronic airway disease that characterizes PCD.[22,23]

We identified a PCD-causing apparent homozygous variant and a compound heterozygous variant in the growth-arrest-specific 2-like 2 (*GAS2L2*; [MIM: 611398], [GenBank: NM_139285.3, 17q12]) in two individuals with symptoms of PCD but with normal axoneme structure. GAS2L2 is a member of the GAS2 family, which includes GAS2, GAS2L1, GAS2L2, and GAS2L3.[24,25] The GAS2 family mediates crosstalk between actin filaments and microtubules (MT). They all contain a calponin homology (CH) domain (a putative actin binding site) and a GAS2-related (GAR) domain (a putative MT binding domain), but only the GAS2-like proteins contain a larger unstructured C terminus that contains the conserved microtubule-tip localization sequences Ser/Thr-Xaa-Ile/Leu-Pro (or SxIP motifs) necessary for interaction with microtubule plus-end-binding (EB) proteins.[25,26] The

[1]Cystic Fibrosis/Pulmonary Research and Treatment Center, University of North Carolina, Chapel Hill, NC 27599, USA; [2]Biology Department, University of North Carolina, Chapel Hill, NC 27599, USA; [3]Department of Cell and Molecular Biology, Feinberg School of Medicine, Northwestern University, Chicago, IL 60611, USA; [4]Department of Medicine, Division of Pulmonary and Critical Care Medicine, University of North Carolina, Chapel Hill, NC 27599, USA; [5]Center for Environmental Medicine, Asthma, and Lung Biology, University of North Carolina, Chapel Hill, NC 27599, USA; [6]Department of Pharmacology, University of North Carolina, Chapel Hill, NC 27599, USA; [7]Assistance Publique-Hôpitaux de Paris, Service de Pneumologie et Allergologie Pédiatriques, Hôpital Necker-Enfants Malades, Université Paris Descartes, Paris 75015, France; [8]Sorbonne Université, Institut National de la Santé et de la Recherche Médicale, Childhood Genetic Disorders, Département de Génétique Médicale, Assistance Publique-Hôpitaux de Paris, Hôpital Trousseau, Paris 75012, France; [9]Department of Pathology and Laboratory Medicine, University of North Carolina, Chapel Hill, NC 27599, USA
[10]These authors contributed equally to this work
*Correspondence: ostro@med.unc.edu (L.E.O.), maimoona_zariwala@med.unc.edu (M.A.Z.)
https://doi.org/10.1016/j.ajhg.2018.12.009.

GAS2 [MIM: 602835] is expressed in many human tissues[27] and is involved in the regulation of microfilament dynamics during both the cell cycle and apoptosis.[28,29] The overexpression of *GAS2* is a hallmark in myeloid leukemia,[30] and its absence has been related to infertility due to follicle growth impairment in mice.[31] *GAS2L1* [MIM: 602128] is also expressed in multiple human tissues.[24] It localizes to the proximal end of mature centrioles and participates in centriole dynamics and centrosome disjunction,[32] inhibits the growth of red blood cells downstream of thyroid receptor signaling,[33] and is downregulated in myeloid leukemia.[34] *GAS2L3* [MIM: 617224] is expressed in many cell types.[35] It is essential for brain morphogenesis and development[36] and might play a role in tumorigenesis.[37] *GAS2L2* has six exons, encodes a 97 kDa protein, and is the least characterized member of the family. Previous studies showed that GAS2L2 localized with both actin stress fibers and microtubules and thereby contributed to different levels of actin-microtubule co-alignment.[25] A separate study showed that the transfection of *GAS2L2* into HEK293 cells stabilized the interaction of the A_{2A} adenosine receptor with the Gsα subunit, increasing the cellular cAMP content.[38] However, little is known about the localization and function of GAS2L2 in native tissues. We sought to determine the expression and localization of GAS2L2 specifically in airway cells, and its role in PCD development. In normal airway ciliated cells, GAS2L2 localizes throughout the cytoplasm but is abundant near basal bodies. In human and mouse airway cell cultures, the absence of *GAS2L2* impaired ciliary orientation, and the ciliary beat was hyperactive and uncoordinated. Similarly, in *X. laevis* the absence of *Gas2l2* disrupted cilia rotational polarity. Knockout of *Gas2l2* in mice resulted in neonatal death. Adult *Gas2l2*-conditional-KO mice developed a PCD phenotype with impaired nasal MCC. These results demonstrate that defective ciliary orientation, resulting from a genetic variant in *GAS2L2,* causes PCD.

Material and Methods

Subjects

Individuals included in the study had a clinical diagnosis of PCD confirmed by standard clinical diagnostic criteria. For studies of affected individuals and their families, all individuals gave their signed and informed consent. All protocols involving human studies were approved by the University of North Carolina Medical School Institutional Review Board and the Ethics Review Board of the Comité de Protection des Personnes CPP Ile-de-France III (France) (approvals no. CPP07729 and CPP02748).

Genetic Analysis

Identification of *GAS2L2* variants was performed either by whole-exome sequencing as previously described[39] or by parallel sequencing with a custom targeted-capture panel encompassing 38 genes implicated in PCD (Table S1) and 250 candidate genes (SeqCap EZ Choice, Roche Diagnostics; details available on request). Copy-number-variation analysis was performed with a depth-ratio comparison between the individuals sequenced in the same run. Performing Sanger sequencing (Life Technologies) validated the genetic *GAS2L2* variants found in the affected individuals. Segregation analysis was performed on the available DNA from family members (UNC-362). The primers used are listed in Table S2. More than 455 unrelated individuals suspected of having PCD were screened for biallelic genetic variants in *GAS2L2* by various methodologies, including whole-exome sequencing, panel testing, and Sanger sequencing.

Airway Epithelial Cell Cultures

Human bronchial epithelial (HBE) cells were obtained from male and female, non-smoking donors lacking respiratory pathologies. The HBE cells were provided by the Cystic Fibrosis Center Tissue Procurement and Cell Culture Core under protocols approved by the University of North Carolina (UNC) Medical School Institutional Review Board. HBE cells were cultured at the air/liquid interphase (ALI) as previously described.[40]

Human nasal epithelial (HNE) cells from proband PCD-1367 and controls were obtained as described.[41] The nasal cells were expanded as conditionally reprogrammed cells (CRCs).[42] In brief, irradiated 3T3J2 fibroblasts were seeded on collagen-coated culture dishes 12 hr before coculture with HNE cells in CRC media supplemented with 5 μM of the Rho-associated kinase (ROCK) inhibitor (Y-27632, Sigma SCM075). To induce cell differentiation, we seeded cells in collagen-coated Millicell inserts (Millipore) and cultured at the air-liquid interface.

Mouse trachea epithelial cells (mTECs) were isolated according to established protocols.[43] Tracheas were dissected from adult mice or 18.5 days post-coito (dpc) embryos. The cells were expanded and cultured as described above.

Reverse-Transcription Polymerase Chain Reaction

Semiquantitative reverse-transcription polymerase chain reaction (RT-PCR) for detection of *GAS2L2* was performed via standard protocols. In brief, total RNA from human tissues was obtained from Takara Bio (Takara Bio). Total RNA from wild-type mouse tissues and from airway epithelial cell cultures (human and mouse) were isolated with an RNeasy kit (QIAGEN) according to the manufacturer's protocols. First-strand cDNA was synthesized with SuperScript II Reverse Transcriptase (Thermo Fisher cat.# 18064014). PCR was performed with PrimeSTAR HS DNA Polymerase (Takara Bio) according to the manufacturer's protocols. For the normalization of RT-PCR analysis of human tissues, *PPIA* (*cyclophilin A*) was used as a reference[44] and *DNAI1* as a control of ciliogenesis progression. RT-PCR analysis of mouse tissues was normalized with TATA box protein (*Tbp*) and β-actin (*Actb*).[45] The primers used are listed in Table S3.

Immunofluorescence and Co-localization Analysis

Immunofluorescence was performed as described previously.[46] For whole-mount staining, ALI cultures were washed with PBS and fixed with 4% paraformaldehyde for 20 min at room temperature, permeabilized with 0.2% Triton X-100 in Tris-buffered saline for 30 min, and then incubated for 1 hr at room temperature in blocking solution (1% BSA, 1% fish gelatin, 0.1% Triton X-100, and 5% fetal bovine serum). After primary antibody incubation, antibody binding was detected with secondary antibodies conjugated with Alexa Fluor-488, Alexa Fluor-647 (Life Technologies), indocarbocyanine- (CY3), or Rhodamine Red-X (RRX) (Jackson ImmunoResearch Laboratories). Actin filaments were stained

with phalloidin conjugated with Alexa Fluor 488 (Life Technologies A12379). For DNA staining, Hoechst 33342 trihydrochloride, trihydrate-FluoroPure (Life Technologies) was used. No detectable staining was observed for isotype-matched control antibodies. Membranes were mounted on slides with ProLong Diamond antifade mountant (Thermo Fisher). The antibodies used are listed in Table S4. Whole-mount ALI cultures were imaged with a Leica SP8 inverted confocal or a Nikon N-SIM microscope. Single cells were imaged with a Nikon N-SIM microscopy system. Images were processed and analyzed with FIJI.[47] For co-localization analysis, single cells were embedded in 100 mM β-mercaptoethylamine (Sigma) for ground-state depletion (GSD) super-resolution microscopy (Leica). So that Pearson coefficients (r: values between −1 to 1; where −1 = inverse association and 1 = full association) and Manders coefficients for magenta (M_1) and green (M_2) channels (M_1 and M_2; values vary from 0–1, where 0 = no overlapping and 1 = 100% co-localization)[48] could be obtained, images were analyzed with the Coloc2 plugin of ImageJ[49].

Immunoblots and Targeted Proteomics Analysis

Human nasal epithelial cells were lysed in RIPA buffer (Thermofisher) supplemented with protease inhibitor cocktail (Sigma). Protein concentration was determined via the BCA method (Pierce BCA kit, ThermoFisher Scientific). The samples (20 μg) were electrophoresed on NuPage 4–12% Bis-Tris gels in MES-SDS running buffer (ThermoFisher Scientific) and transferred to 0.45 μm nitro-cellulose membrane for immunoblotting. Targeted proteomics is described in the Supplemental Data. The antibodies used are listed in Table S4.

Analysis of Ciliary Function

Ciliary beat frequency was measured as previously described.[50] In brief, three to four cultures were individually visualized with a Nikon Eclipse TE2000 inverted microscope with phase optics and a 20× objective (NA = 0.45). The temperature was maintained at 37°C via a Tokai HIT controller (model INU-TIZ-F1) and a microscope stage-heater block. High-speed videos (60 frames/s) were recorded with a Basler acA1300-200um camera controlled by SAVA software (Ammons Engineering) and were analyzed via SAVA whole-field analysis. For evaluation of the waveform and beat direction, high-resolution videos of ciliated cells were recorded at 200 fps with a 60× Plan-Apo oil objective lens (NA = 1.4), DIC optics, and ambient temperature. Analysis of videos was conducted by investigators blinded to the cells' genotype. Videos were replayed in slow motion (1/7 of the true speed). For waveform analysis, three cilia were traced manually at the end recovery and end effective positions in four ciliated cells from each genotype. To evaluate the direction of the ciliary beat, we manually traced the tip positions of four to five individual cilia, and the orientation of the ciliary beat was represented in a two-dimensional plot.

Transmission Electron Microscopy and Scoring of Ciliary Orientation

Fixed cultures were sectioned (1 μm) and stained.[51] From three biological replicates, 10 to 15 images of individual cells were taken with a Zeiss 900 TEM at 10,000×. So that ciliary orientation could be scored, the angle (0°–360°) between the center of the basal body to the tip of the basal foot was determined with ImageJ. The length of the mean vector (r)[52] and the average of the length of the mean vector (R) for each genotype were calculated. The mean vector lengths were plotted with Oriana 4. The R values were plotted with GraphPad Prism 7.1 and compared via a Student's t test.

Transgenic *Gas2l2* Mice

All protocols were approved by the University of North Carolina at Chapel Hill (UNC) Institutional Animal Care and Use Committee (IACUC). A knockout-first $Gas2l2^{tm1a(KOMP)Wts/i/+}$ ($Gas2l2^{+/-}$) mouse in a C57BL/6N; C57BL/6N-$A^{tm1Brd/a}$ background was acquired from the Wellcome Trust Sanger Institute knockout mouse project (KOMP).[53] After several unsuccessful attempts at breeding, the mouse was euthanized, and *in vitro* fertilization was used for generation of the $Gas2l2^{+/-}$ line in the same genetic background. $Gas2l2^{fl/fl}$ mice were generated from a cross of $Gas2l2^{+/-}$ mice to a *Rosa26::FLPe* mouse (Jackson Laboratory stock no.: 003946) so that the *lacZ* and *neo* cassettes were removed. The $Gas2l2^{fl/fl}$ mice therefore contain loxP sites flanking exon 2 of *Gas2l2*. Tamoxifen inducible *Gas2l2* conditional-knockout (*Gas2l2* conditional-KO) mice were obtained by crossing $Gas2l2^{fl/fl}$ mice to $Rosa^{CreER}$ mice (Jackson Laboratory stock no.: 004847) or to $Foxj1^{CreERT2::GFP/+}$ mice (Jackson Laboratory stock no.: 027012).[54] Treatment with tamoxifen activates Cre and causes the deletion of exon 2. Primers used for genotyping are listed in Table S3.

Tamoxifen Treatment and CT-Scan Analysis

For all studies, $Gas2l2^{fl/fl}$:$Foxj1^{CreERT2::GFP/+}$ ($Gas2l2^{fl/fl}$:$Foxj1^{CreERT2}$) and control animals were treated with tamoxifen[55] (dissolved in pure corn oil at 20 mg/mL; Sigma-Aldrich). Animals received three intraperitoneal injections of tamoxifen (75 mg/kg body weight) every other day so that the initial deletion of *Gas2l2* would be induced, and thereafter they were maintained on a tamoxifen-supplemented diet (Envigo TD.130860). In most experiments, *Gas2l2* conditional-KO animals were compared to litter mate control mice of genotypes $Gas2l2^{fl/fl}$ or $Gas2l2^{fl/+}$:$Foxj1^{CreERT2}$. For evaluation of the development and progression of the PCD phenotype, the nasal cavity of the mice was scanned by micro-computed tomography (micro-CT) four times, starting at the end of the last tamoxifen injection (baseline) and repeating every 30 days. Micro-CT scans were analyzed with Mimics Research 18.0, and the volume of the nasal air space (V) was calculated. The change in nasal air space (ΔV) was calculated by subtracting the baseline nasal air space ($V_{baseline}$) from the volume measured at 90 days (V_{90}).

Measurement of MCC

For measurement of MCC in the nasal cavity and in the anterior nasopharynx, the clearance of radiolabeled ^{99m}technetium colloid particles[56] or dry green-fluorescent beads,[57] respectively, was recorded. Analyses were performed using ImageJ[48] and Mosaic plugin.[58]

Histology of the Nasal Cavity

After measurement of MCC, the heads of the mice were fixed and processed as previously described.[59] Coronal sections of the nasal cavity were stained with hematoxylin and eosin (H&E) and with alcian blue and periodic acid Schiff (AB-PAS) stain so that mucus accumulation could be visualized. For comparisons between genotypes, the samples were screened for the presence of mucus and for degeneration of the epithelium. The presence of mucus was scored from one to four as previously described.[59] Images were taken with an Olympus VS120 virtual slide scanner microscope.

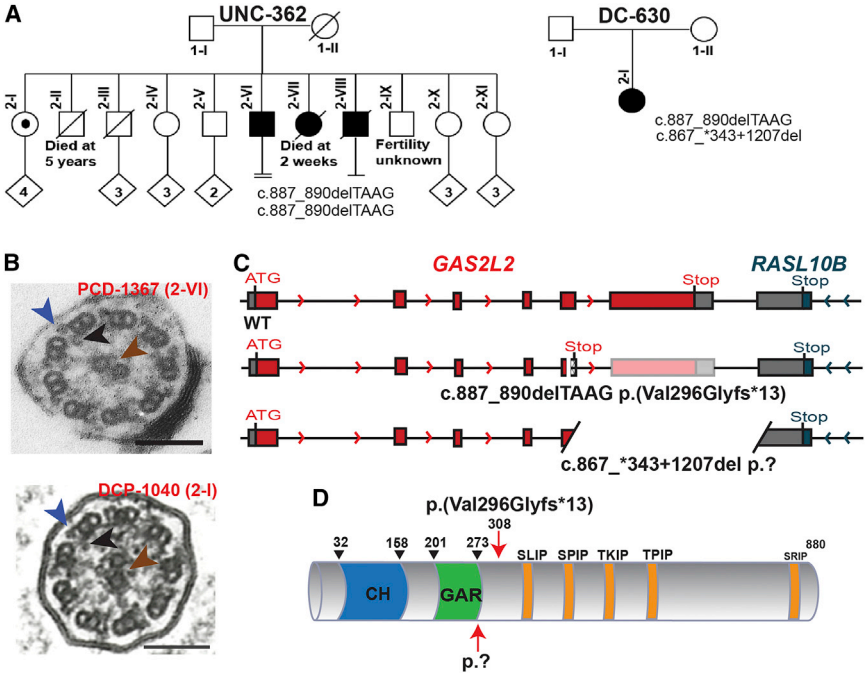

Figure 1. *GAS2L2* Pathogenic Variants in Individuals with PCD

(A) Segregation analysis of *GAS2L2* genetic variants found in family UNC-362 (c.887_890delTAAG [p. Val296Glyfs*13]) and in family DC-630 (c.887_890delTAAG; 867_*343+1207del [p.Val296Glyfs*13;?]). Filled symbols indicate PCD-affected individuals. In family UNC-362, individual 2-I is a heterozygous carrier, individual 2-II died at age 5 years as a result of a ruptured appendicitis. Individual 2-III was a lifelong smoker and died of lung cancer at ~55 years. Individual 2-VI is proband PCD-1367. Individual 2-VII was a term neonate suspected to have had PCD as a result of neonatal respiratory distress and severe hypoxemia. She died at 2 weeks. Individual 2-VIII is suspected to have had PCD as a result of phenotypic features including daily cough and bronchiectasis at age 10 years with subsequent lobectomy. He passed away from lymphoma at 50+ years.

(B) A transmission electron micrograph of axonemal cross sections of nasal epithelium from both probands shows the central pair (brown arrowhead) surrounded by nine microtubule doublets. Outer dynein arms (blue arrowhead) and inner dynein arms (black arrowhead) project from each doublet normally.

(C) Schematic representation of the *GAS2L2* variants found in the PCD-affected individuals. The top panel shows normal exon-intron structure, the middle panel shows the small four-nucleotide deletion (c.887_890del) that introduces an early stop codon, and the bottom panel shows the large deletion (c.867_*343+1207del) that is also located in exon 5. Red boxes indicate the coding exons, patterned boxes indicate out-of-frame sequence, and gray boxes indicate the 5′ and 3′ UTRs.

(D) Schematic representation of GAS2L2 structure. It contains a calponin homology (CH, blue) domain and a GAS2-related domain (GAR, green), which might mediate binding to the actin cytoskeleton and MT, respectively. Conserved SxIP motifs for interaction with EB proteins are indicated in orange. The location of the mutations is indicated by the red arrows. The small deletion induces a frameshift variant that introduces a stop codon in amino acid 308. The large deletion disrupts the protein after the GAR domain.

Xenopus laevis Embryo Manipulation and Analysis

Xenopus embryos were obtained by *in vitro* fertilization according to standard procedures.[60] All protocols were approved by the UNC IACUC committee. The *X. laevis* genome contains two largely identical *Gas2l2* copies that have different start codons. Two separate morpholinos (Table S3) targeting the start codon of each isoform were designed on the basis of the sequences from the NIBB database and obtained from Gene Tools. To deplete both isoforms simultaneously, *Gas2l2* morpholinos (*Gas2l2*-MO) were injected together at 20-60 ng/blastomere into the two ventral cells at the four-cell stage so the ciliated epidermis was targeted. Coinjection of *Centrin 4-RFP* mRNA (Unigene ID: Xl.50473) and *Clamp-GFP* mRNA (Unigene ID: Xl.26316) labeled basal bodies and ciliary rootlets, respectively. For immunostaining and confocal imaging analysis, *X. laevis* embryos at stage 28 were processed as previously described.[61] Antibodies anti-γ-tubulin and anti-Gas2l2 were the same as described above. All imaging of *X. laevis* ciliated cells was performed on a Nikon A1R laser scanning confocal microscope with a 60× oil plan-Apo objective lens (1.4 NA). Cilia orientation was scored as previously described.[62] In brief, individual rootlet orientation was scored manually by measurement of the angle of orientation of the rootlets relative to the anterior–posterior axis of the embryo. Mean vector-length calculations and graphical representation of cilia orientation via circular plots were performed with Oriana 4.02 software.

Statistical Analysis

Data are expressed as the mean ± standard deviation (SD) of n experiments. In these studies, we used the following statistical methods: two-tailed Student's t test with Welch's correction, Paired t test, one-way ANOVA with Tukey's multiple comparisons, chi-square test, and Pearson's correlation test. Figure legends specify the statistical method used for each experiment. P values less than 0.05 were considered significant.

Results

Discovery of Genetic Variants in *GAS2L2*

Although genetic variants in more than 40 genes have been identified as causes of PCD,[1,4–8] in many cases of PCD the genetic lesion has not yet been identified. To uncover additional variants that cause PCD, we performed whole-exome sequencing of a subject with clinical features consistent with PCD (Table S5). We identified an apparent homozygous frameshift variant, c.887_890delTAAG (p.Val296Glyfs*13) (dbSNP: rs587633197) in exon 5 of *GAS2L2* (GenBank: NM_139285.3) (Figures 1A and S1A). Proband PCD-1367 from family UNC-362 (2-VI) was diagnosed at the age of 56 years. DNA from the parents was not available; however, subject 2-I is a

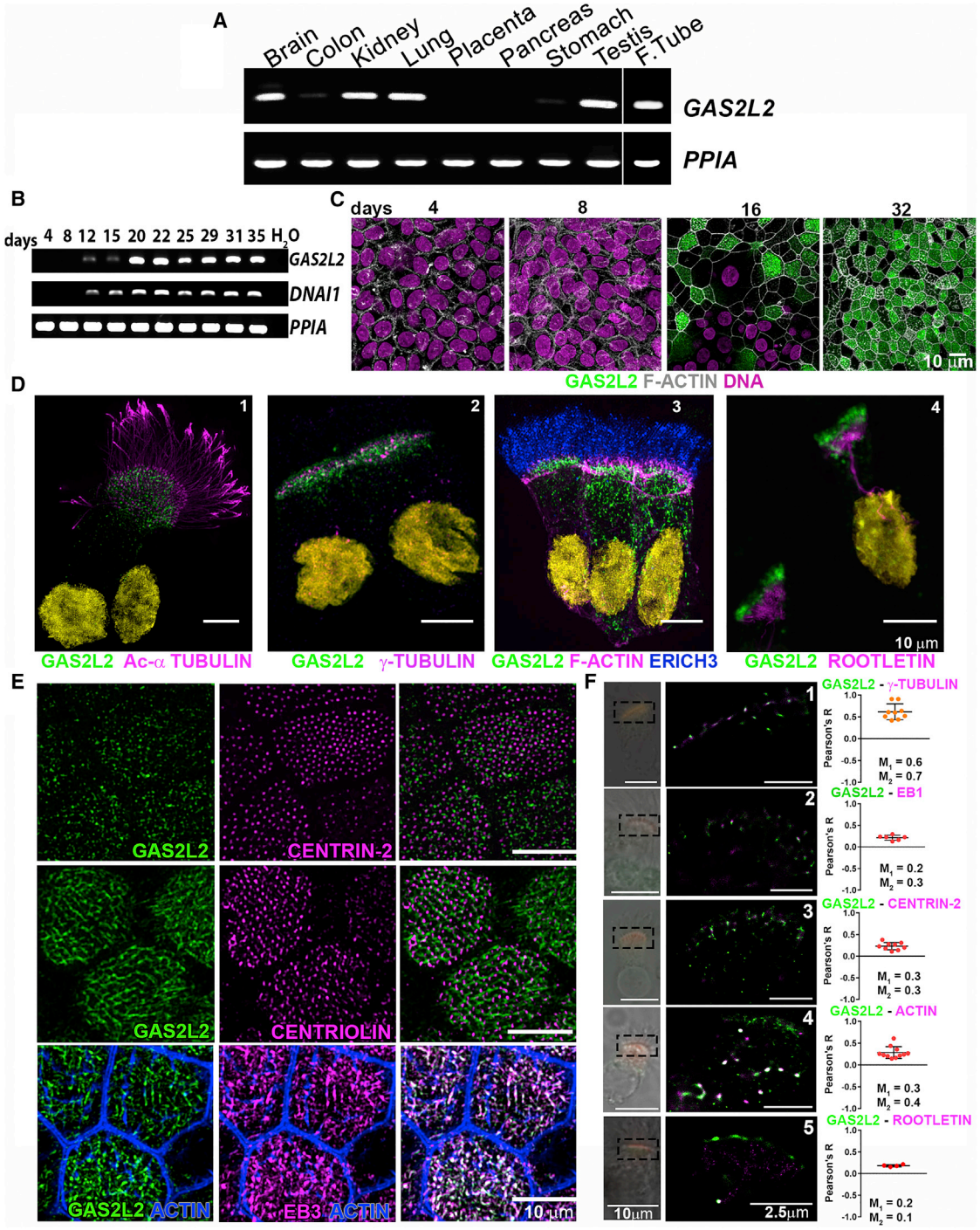

Figure 2. Expression and Localization of GAS2L2

(A) Total RNA from different human tissues was used for determining the expression of *GAS2L2*. *PPIA* was used as a reference.

(B) Expression of *GAS2L2* in normal HBE cells. Total RNA was extracted at the different indicated days of ALI culture. The expression of *GAS2L2* correlated with the expression of *DNAI1*, a ciliated-cell-specific gene. *PPIA* was used as a reference.

(C) Whole-mount immunofluorescence. HBE cultures were fixed at different days during the differentiation of airway cells and stained for actin filaments (gray) and GAS2L2 (green), and nuclei (magenta) were labeled with Hoechst 33342. GAS2L2 was not detected in undifferentiated cells (days four through eight). It was observed in the cytoplasm of HBE cells (day 16), and it was strongly present in fully differentiated cultures (day 32).

(D) Isolated cell immunofluorescence. Cells were stained for GAS2L2 in green and in magenta: (1) the ciliary axoneme marker Acetylated-αtubulin; (2) basal-body marker γ-tubulin; (3) actin filaments and ERICH3 (blue), a ciliary axoneme marker; and (4) the rootlet marker rootletin. Nuclei (yellow) were labeled with Hoechst 33342.

(E) Whole-mount culture immunofluorescence. GAS2L2 is closely associated with centrin-2 (top panel) and centriolin (middle panel). GAS2L2 strongly localizes with EB3 (bottom panel).

(legend continued on next page)

heterozygous carrier, and the family history suggested that two other siblings were affected by PCD (Figure 1A); these included a sister who had neonatal respiratory distress and severe hypoxemia and died at 2 weeks and a brother who had a daily cough and bronchiectasis and underwent a lobectomy. During the course of this research, a second individual with a compound heterozygote genetic variant in *GAS2L2* was identified (Figure 1A). Proband DCP-1040 (2-I) from family DC-630 carries the same c.887_890delTAAG (p. Val296Glyfs*13) frameshift variant and a large deletion (c.867_*343+1207del p.?) (LOVD: 0000439768] starting in exon 5 (Figure S1B). DNA from the parents was not available, and they had no report of upper or lower chronic respiratory disease. The location of the two deletions that proband DCP-1040 carries indicates that she is an obligatory compound heterozygote. Indeed, within *GAS2L2* exon 5, the 5′ breakpoint of the large deletion c.867_*343+1207del (with a 3′ breakpoint in the adjacent gene *RASL10B* and, therefore, encompassing *GAS2L2* exon 6) is upstream of the small four-nucleotide deletion c.887_890del, also located in exon 5. Next-generation sequencing (NGS) data (Figure S2A) highlights the absence of a normal allele for exon 5 because reads either include c.867_*343+1207del or c.887_890del. Additionally, copy-number analysis based on NGS read depth (Figure S2B) confirmed the heterozygous deletion of exon 6 and the partial heterozygous deletion of exon 5. Both individuals have similar clinical phenotypes, including bronchiectasis, otitis media, and rhinosinusitis (Table S5). However, the ultrastructure of the ciliary axoneme was normal (Figure 1B), and one of the individuals had normal levels of nasal NO (nNO = 342.6 nL/min, cutoff 77 nL/min)[63] (Table S5). The *GAS2L2* genetic variants that we identified in the PCD-affected families (Figure 1C) are both predicted to result in the absence of protein production as a result of immature full-length transcripts and/or nonsense-mediated mRNA decay. GAS2L2 possesses a GAS2-related (GAR) domain for interacting with microtubules and a calponin homology (CH) domain for interacting with actin filaments.[24,25] Interestingly, GAS2L2 has a long C terminus with five putative SxIP sites for interaction with microtubule-end-binding (EB) proteins (Figure 1D). The frameshift variant induces a stop codon in amino acid 308, after the microtubule-binding domain (Figure 1D). The large deletion (3,931 nucleotides) might disrupt the putative protein after the GAR domain (Figure 1D). Because of these findings, we sought to determine the expression and localization of GAS2L2 specifically in airway cells and its possible role in PCD development.

GAS2L2 Is a Ciliated-Cell-Specific Protein

In control human tissues, *GAS2L2* transcript was abundant in tissues with motile cilia; including brain, lung, testis, and fallopian tube. *GAS2L2* expression was also detected in kidney tissue, and less abundantly in stomach and colon tissue (Figure 2A). To determine the expression and localization of *GAS2L2* during HBE cell differentiation, we used RT-PCR and immunofluorescence, respectively (Figures 2B and 2C). The expression of *GAS2L2* was not detected in undifferentiated cells. By day 12 of ALI culture (Figure 2B), we observed a weak *GAS2L2* signal correlating with the expression of *DNAI1* [MIM: 604366]. At later time points, *GAS2L2* was strongly expressed in a similar pattern to that of *DNAI1* (Figure 2B), and the protein was abundant in the cytoplasm of HBE cells (Figure 2C). In single-cell immunostaining, GAS2L2 strongly localized at the base of the cilia (Figure 2D-1), close to γ-tubulin (a basal body marker, Figure 2D-2). Also, GAS2L2 was detected in the cytoplasm of ciliated cells, and it partially localized with actin filaments (Figure 2D-3) and rootletin (a rootlet marker; Figure 2D-4). In whole-mount cultures (Figure 2E), we confirmed the cytoplasmic localization of GAS2L2 with centrin-2 (Figure 2E, top panel) and centriolin (basal feet marker, Figure 2E, middle panel) at the base of the cilia. GAS2L2 also localized with EB3 (Figure 2E, bottom panel), an interaction previously described.[25] GAS2L2 was not detected in secretory cells labeled with CC10 and MUC5B (Figures S3A and S3B). Co-localization analysis showed that GAS2L2 co-localizes with γ-tubulin (Pearson's coefficient, $r = 0.62 \pm 0.18$; Manders coefficients, $M_1 = 0.6$, $M_2 = 0.7$; Figure 2F-1) and partially co-localizes with EB1 ($r = 0.21 \pm 0.06$; $M_1 = 0.2$, $M_2 = 0.3$, Figure 2F-2), centrin-2 ($r = 0.23 \pm 0.08$; $M_1 = 0.3$, $M_2 = 0.3$; Figure 2F-3), and actin ($r = 0.28 \pm 0.14$; $M_1 = 0.3$, $M_2 = 0.4$; Figure 2F-4) but not with rootletin ($r = 0.18 \pm 0.02$; $M_1 = 0.2$ and $M_2 = 0.1$; Figure 2F-5). These results suggest that GAS2L2 interacts closely with proteins present at the basal body.

The Loss of *GAS2L2* Disrupts Cilia Beat Frequency and Orientation

To investigate the functional role of GAS2L2 in ciliated cells, we cultured HNE cells from the proband PCD-1367 (*GAS2L2*-deficient) and control cells and expanded them as CRCs.[42] (Figure 3A). The screening of *GAS2L2*-deficient cells by immunoblot and immunofluorescence showed complete absence of GAS2L2 (Figures 3B and 3C). Also, a truncated form of the protein was not detected by targeted proteomics (Figure S4A and Table S6; see also Supplemental Methods). In PCD-1367 cells, the transcript of *GAS2L2* was reduced (Figure S4B), possibly as a result of

(F) Single-molecule detection using GSD super-resolution microscopy showing representative images of cells stained with GAS2L2 (green) and in magenta: (1) γ-tubulin, (2) EB1, (3) centrin-2, (4) actin, and (5) rootletin. The boxed area in the bright-field image was scanned in GSD mode. Pearson coefficients for each analyzed cell are represented in the graph ($n \geq 4$). The average Manders coefficient for GAS2L2 (M_1) and the partner protein (M_2) are indicated.

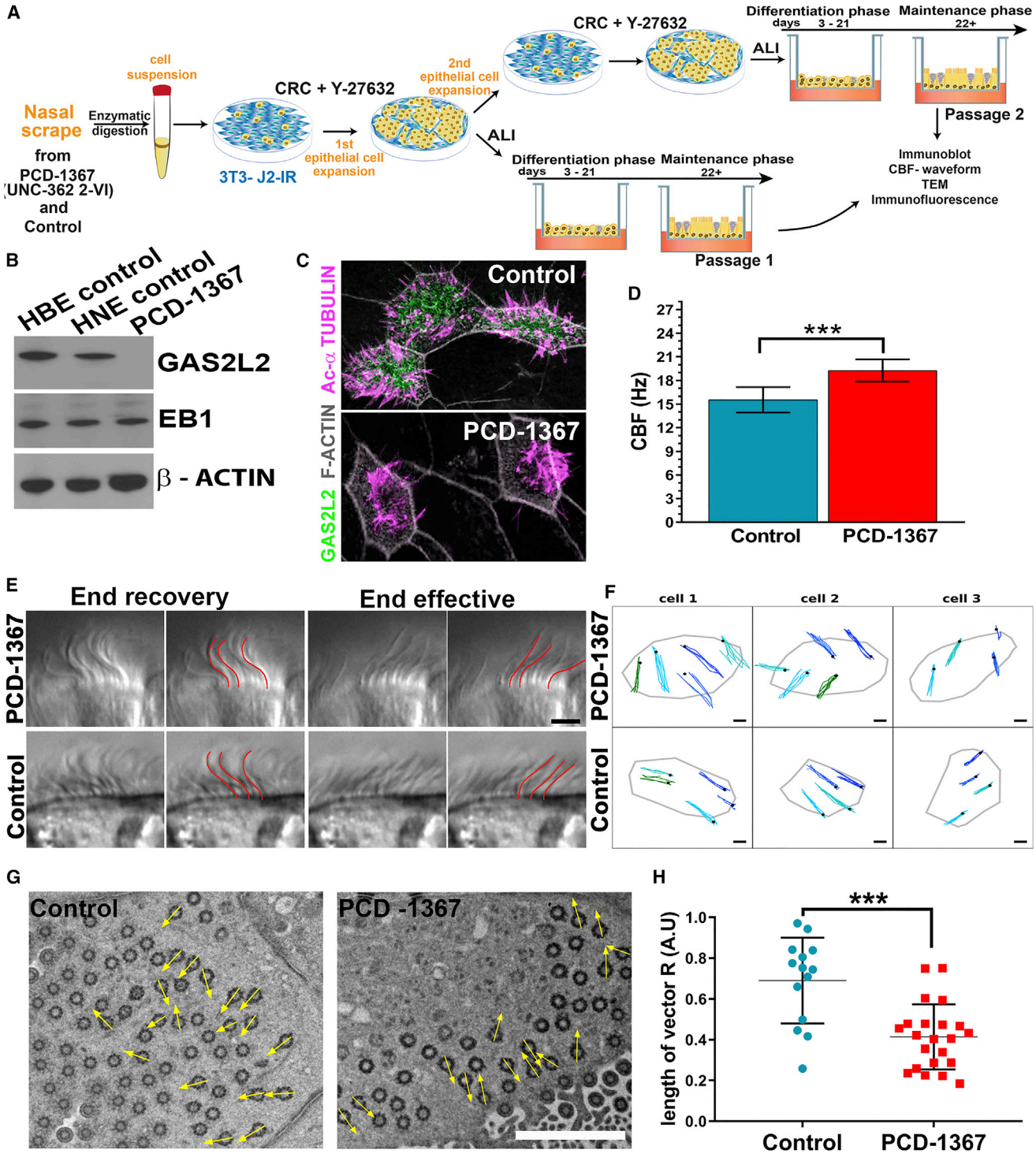

Figure 3. The Absence of GAS2L2 Causes a Defective Ciliary Beat

(A) Nasal epithelial cells from individual PCD-1367 (family UNC-362, 2-VI) and a control were dissociated into single cells. The HNE cells were conditionally reprogramed and expanded by co-culture with irradiated 3T3J2 fibroblasts for one to two passages in the presence of Y-27632, a selective inhibitor of Rho-associated protein kinase (ROCK). After expansion, we cultured the HNE cells at the ALI to conduct multiple assays.

(B and C) The absence of GAS2L2 in PCD-1367 was confirmed by immunoblot and immunofluorescence.

(D) The CBF in *GAS2L2*-deficient cells was hyperkinetic in comparison to controls (n = 6; data are represented as the mean + SD; Student's t test, ***p = 0.0002).

(E) High-resolution videos of ciliated cells were observed and showed a normal waveform pattern of ciliary beat in control and *GAS2L2*-deficient cells. The images represent a time point of the cilia seen in profile at end recovery (left panels) and end effective positions (right panels). For each position, a panel showing the manual tracing of the cilia (highlighted in red) is shown. (n = 4; the scale bar represents 4 μm).

(legend continued on next page)

nonsense-mediated decay of the mRNA. The ciliary beat frequency (CBF) was significantly faster in *GAS2L2*-deficient (19.8 ± 0.2 Hz) cells than in control cells (15.8 ± 0.1 Hz; p = 0.0002; Figure 3D). Although the waveform appeared normal in ciliated cells from proband PCD-1367 (Figure 3E, additional traces are shown in Figure S5 and Videos S1 and S2), the direction of the ciliary beat appeared to be randomized (Figure 3F, top panel; also Video S3) in comparison to control cells (Figure 3F, bottom panel; also Video S4). To further analyze the coordination of the ciliary beat, we measured the orientation of the basal feet in individual ciliated cells. In cell culture, the direction of the ciliary beat varies between cells, but it is well coordinated within individual cells; however, in *GAS2L2*-deficient cells the alignment of the basal feet was significantly randomized (Figure 3G). The length of the mean vector (r) was shorter in the *GAS2L2*-deficient cells (r = 0.05) than in control cells (r = 0.469). This was further reflected by a low average length of the mean vector (R) for *GAS2L2*-deficient cells compared to control cells (0.41 + 0.034 versus 0.65 + 0.065; p < 0.001, Figure 3H). These results demonstrate that the absence of *GAS2L2* in human airway ciliated cells causes a ciliary orientation defect and affects the performance of the cilia.

Deletion of *Gas2l2* Causes Neonatal Lethality in a Mouse Model

To analyze the function of GAS2L2 *in vivo*, we used a *Gas2l2*-knockout-first mouse (*Gas2l2*$^{tm1a(KOMP)Wtsi}$ or *Gas2l2*$^{+/-}$) (Figure 4A). More than 90% of the *Gas2l2*$^{+/-}$ mice survived, and they had no signs of a PCD phenotype. Because in mouse, as in humans, the localization of *Gas2l2* expression is largely unknown, we took advantage of the presence of the *lacZ* reporter in *Gas2l2*$^{+/-}$ mice and detected β-galactosidase activity in tissues with motile cilia; such tissues included those of the brain, nasal septum, trachea, lungs, and testis (Figure S6A). RT-PCR corroborated these results (Figure S6B). Matings between heterozygous *Gas2l2*$^{+/-}$ mice resulted in a high incidence of neonatal death (~29%). Of the 265 mice that survived, only two were *Gas2l2*$^{-/-}$ (Figure 4B). These mice showed signs of hydrocephalus at 14 and 21 days of age. Histology of the head (Figure 4C) showed mucus accumulation in multiple sinuses and remodeling of the nasal cavity, a typical phenotype of murine PCD models (e.g., *Dnaic1*$^{-/-}$ mice).[59] To evaluate inheritance ratios, we genotyped 18.5 dpc embryos; ~13% (6/48) were homozygous ($x^2_{obs} = 6.00$, with 2 degrees of freedom; p = 0.05; Figure S6C), consistent with Mendelian distribution. Of the six *Gas2l2*$^{-/-}$ embryos collected, three showed dextrocardia (Figure 4D), suggesting that *Gas2l2* is expressed in ciliated cells at the node and might play a role in situs determination.

Deletion of *Gas2l2* in mTEC Cultures and in *X. laevis* Embryos Recapitulates the Ciliary Phenotype Observed in Humans

To further investigate the role of GAS2L2 in ciliary function, we used two vertebrate models: the knockout mouse and *X. laevis* embryos. In wild-type cells from both species, GAS2L2 localized at the base of the cilia, near the basal bodies (Figures 5A and 6A). To investigate the effects of *Gas2l2* deletion, we cultured mTEC isolated from embryonic tracheas. We pooled tracheas of the same genotype, digested them to obtain a single cell suspension, expanded them as CRC cells, and then cultured them at an ALI until they were differentiated. The absence of *Gas2l2* was confirmed by RT-PCR (Figure S7A). The CBF of *Gas2l2*$^{-/-}$ mTEC was hyperkinetic (24.71 ± 1.28 Hz) in comparison to controls (*Gas2l2*$^{+/+}$ = 18.77 ± 0.94 Hz, Figure 5B and *Gas2l2*$^{+/-}$ = 20.57 ± 0.80 Hz; data not shown). We observed a lack of alignment of the basal feet within individual *Gas2l2*$^{-/-}$ cells (r = 0.40; R = 0.46 ± 0.08) compared to *Gas2l2*$^{+/+}$ cells (r = 0.60; R = 0.71 ± 0.06, Figures 5C and 5D) and *Gas2l2*$^{+/-}$ cells (r = 0.51; R = 0.76 ± 0.036; data not shown). The distribution and spacing of the basal bodies were similar between the *Gas2l2*$^{-/-}$ and the wild-type cells (Figure 5E).

The multiciliated skin cells of *X. laevis* embryos generate a robust flow oriented from anterior to posterior. *X. laevis* expresses two isoforms of *Gas2l2*; therefore, morpholinos (MO) targeting both isoforms were injected into embryos (*Gas2l2*-MO embryos). To visualize and score the orientation of individual cilia, the embryos were co-injected with *Centrin 4-RFP* (rootlet marker) and *Clamp-GFP* (basal-body marker) mRNA.[61] The targeting of *Gas2l2* resulted in mosaic embryos (Figure S7B). The decreased levels of *Gas2l2* affected the number and distribution of basal bodies on the surface of ciliated cells (Figures 6B and 6C). The ciliary orientation was significantly reduced in *Gas2l2*-MO embryos (r = 0.67, CSD = 51.2°) compared to controls (r = 0.98, CSD = 11.5°; Figures 6B′ and 6C′). This phenotype was rescued when human *GAS2L2* mRNA (*GAS2L2-R*) was co-injected (r = 0.91, CSD = 25.6°; p < 0.0001). In addition, the average of the length of the vectors from ciliated cells in *Gas2l2*-MO embryos was significantly shorter than in control-MO and *GAS2L2-R* embryos (Figure 6D).

(F) Direction of ciliary beat. Four to five cilia were tracked manually in three individual cells. The black dot represents the position at the end recovery phase. The direction of the ciliary beat was plotted on an X-Y graph (the scale bar represents 2 μm).
(G) Representative electron micrograph showing the analysis of alignment of the basal body and basal foot in control cells (n = 14) and *GAS2L2*-deficient cells (n = 22). The arrows in each micrograph are pointing in the direction of the basal foot tip (the scale bar represents 2 μm).
(H) The length of the vector (0 < R < 1) for each cell is represented in the graph. The average length of the vector was significantly shorter in *GAS2L2*-deficient nasal ciliated cells than in control cells (data are expressed as the mean + SD; Student's t test, ***p = 0.0004).

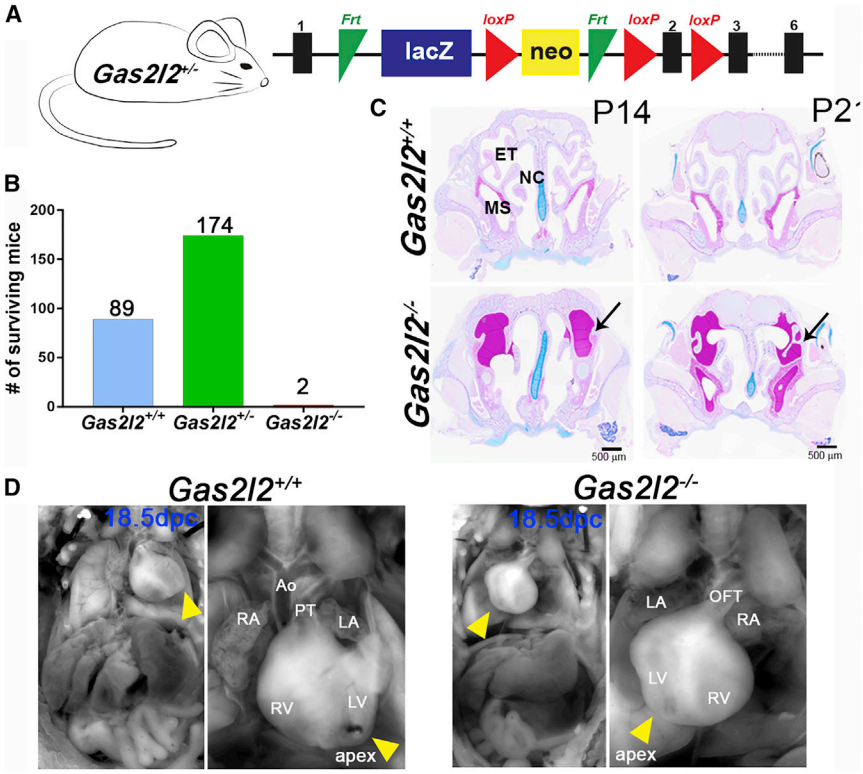

Figure 4. Deletion of *Gas2l2* *In Vivo* Causes a Lethal Trait in Mice

(A) The knockout-first allele contains an IRES:lacZ and a promoter-driven neo cassette inserted into an intron of *Gas2l2*, disrupting *Gas2l2* expression.[53] See Material and Methods for details.

(B) From the $Gas2l2^{+/-}$ × $Gas2l2^{+/-}$ crosses, 265 mice survived; of these, two were homozygous.

(C) Histological head sections of the two $Gas2l2^{-/-}$ and control mice at P14 and P21. The heads were stained with AB-PAS, which revealed severe mucus accumulation in the sinuses of both $Gas2l2^{-/-}$ mice (arrows). Abbreviations are as follows: ET, ethmoturbinates; MS, maxillary sinus; and NC, nasal cavity.

(D) Situs ambiguous was observed in three out of six $Gas2l2^{-/-}$ mouse embryos dissected at 18.5 dpc. Dextrocardia was clearly observed as the apex of the heart (yellow arrow head) was oriented to the right side of the body axis. Abbreviations are as follows: RV, right ventricle; LV, left ventricle; RA, right atrium; LA, left atrium; Ao, Aorta; PT, pulmonary trunk; and OFT, out-flow tract.

Gas2l2 Conditional-KO Mouse Develops a PCD-like Phenotype

To understand the role of GAS2L2 in PCD development, we generated conditional-knockout (KO) mice (Figure 7A). The $Gas2l2^{fl/fl}$ mice were first crossed to a $ROSA26^{CreER}$ mouse. However, we detected by PCR a high incidence of spontaneous deletion of *Gas2l2* (Figure S8A), and most of the $Gas2l2^{fl/fl}$:$Rosa^{CreER/+}$ mice died soon after birth. Tracheal cells from surviving $Gas2l2^{fl/fl}$:$Rosa^{CreER/+}$ and control mice were expanded as CRCs and cultured at ALI. To induce the complete deletion of *Gas2l2*, we treated the cultures with tamoxifen (TMX; 1 µM)[64] and confirmed the deletion by RT-PCR (Figure S8B). The TMX-treated cultures (Figures S8C and S8D) recapitulated the phenotypes observed in *GAS2L2*-deficient HNE cells (Figure 3) and in mTEC cultures from $Gas2l2^{-/-}$ embryonic trachea (Figure 5).

We generated viable conditional-KO ($Gas2l2^{fl/fl}$:$FoxJ1^{CreERT2}$) mice by crossing $Gas2l2^{fl/fl}$ mice to $Foxj1^{CreERT2::GFP/+}$ (knockin/knockout) mice expressing Cre recombinase exclusively in cells with motile cilia. The offspring from this cross had a high rate of neonatal survival (~98%), but we observed isolated cases of hydrocephalus (~3%). Conditional-KO and control animals were injected with TMX and maintained on a TMX- supplemented diet. In a cohort of 41 mice included in these experiments, the TMX-supplemented diet did not affect the weight or survival of the mice. However, this treatment did not completely abolish *Gas2l2* expression in the trachea (Figures 7B and S9).

Mouse models of PCD develop a phenotype characterized by chronic rhinosinusitis and accumulation of mucus in the nasal cavity.[59] To follow the development of rhinosinusitis and mucus accumulation, the nasal cavities of the mice were imaged using micro-CT. The mice were imaged four times at four-week intervals, starting after the third TMX injection (baseline). The CT scans were compared to histological sections (Figure 7C). Of the 21 $Gas2l2^{fl/fl}$:$Foxj1^{CreERT2}$ mice treated with TMX, ~80% developed mucus plugging in multiple nasal cavities and increased nasal air space due to remodeling of the nasal cavity. The nasal air space increased over time and was significant at two and three months after treatment (Figure 7D). These results confirm that the deletion of *Gas2l2* caused a PCD phenotype in mice.

Impaired MCC in *Gas2l2* conditional-KO mice

To directly determine the effect of the deletion of *Gas2l2* on MCC, we used a noninvasive method to monitor in real time the nasal clearance of $Gas2l2^{fl/fl}$:$Foxj1^{CreERT2}$ and control mice.[56] After the intranasal administration of the radioactive tracer Technetium-99 (^{99m}Tc), radioactive particles were observed at the tip of the nose at time 0 (Figure 8A, left panel). These particles were then cleared toward the oropharynx, where they accumulated over time (Figure 8A, central and right panels). The average clearance in *Gas2l2*-conditional-KO mice was significant in comparison to that of $Dnaic1^{-/-}$ mice, which show no MCC (Figure 8B). However, in the *Gas2l2*-conditional-KO mice we observed that the impairment of clearance (with respect to that in control mice) correlated with changes in nasal air space ($\Delta V = V_{90} - V_{baseline}$, Figure 8C, Pearson's $r = -0.7672$, $p < 0.0001$) and the presence of mucus in the

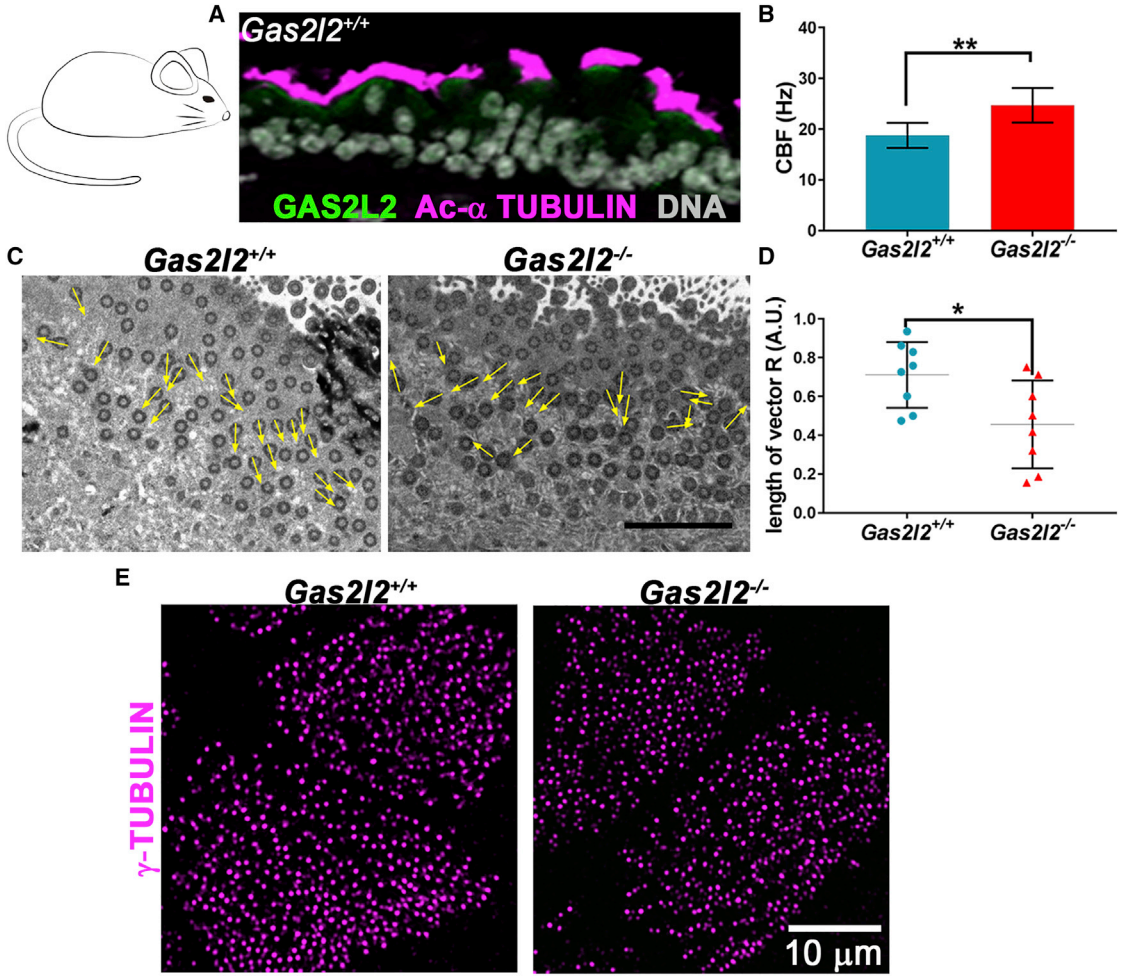

Figure 5. Absence of GAS2L2 in Mouse Tracheal Ciliated Cells Affects CBF and Ciliary Orientation

(A) Detection of GAS2L2 in tracheal ciliated cells from a wild-type mouse by immunofluorescence. Tracheal sections were stained for GAS2L2 (green) and Acetylated-α tubulin (magenta). Nuclei (gray) were labeled with Hoechst 33342.

(B) The CBF in *Gas2l2*$^{-/-}$ mTEC cells was hyperkinetic in comparison to control (n = 9; data are represented as the mean + SD; Student's t test, **p = 0.0033).

(C) Representative electron micrographs showing the analysis of alignment of the basal body and basal foot in cells from *Gas2l2*$^{+/+}$ (n = 8) and *Gas2l2*$^{-/-}$ (n = 8) cultures. The scale bar represents 2 μm.

(D) The length of the vector (0 < R < 1) for each cell is represented in the graph. The average length of the vector was significantly shorter in *Gas2l2*$^{-/-}$ ciliated cells than in control cells (data are expressed as the mean + SD; Student's t test, **p = 0.0232).

(E) Normal distribution of basal bodies in wild-type and *Gas2l2*$^{-/-}$ mTEC cells.

nose. Those mice that had normal clearance had no change in ΔV and no mucus accumulation (five mice), or had ΔV < 5 mm^3 and a mucus-accumulation score of 1 (seven mice). The mice with impaired clearance (nine mice) had ΔV > 5 mm^3 and obvious mucus accumulation (score = 2). Additionally, we measured the clearance of fluorescent microspheres in the nasopharynx at the end of the study. In this technique, which avoids retention of particles in the nasal turbinate, the fluorescent beads were delivered at the ventral wall of the nasopharyngeal (NP) meatus. The effective speed of MCC in *Gas2l2*$^{fl/fl}$*:Foxj1*^{CreERT2} mice (11.63 ± 2.97 mm/sec; n = 21) was significantly slower than that in control mice (13.31 ± 2.17 mm/sec, p = 0.0168, paired t test; n = 20), and the directionality of the flow was significantly affected in *Gas2l2*-conditional-KO mice compared to controls (chi-square x^2 = 1.71; df = 1, Figure 8D, Videos S5 and S6). The beads were transported in various directions, usually at an angle, and the forward movement was intermittent (Figure 8D and Video S6). This phenotype was observed in the 16 mice that had increased nasal air space and mucus accumulation in the nose. These results show that GAS2L2 is necessary for effective MCC in the mouse upper airways.

Discussion

We have identified two unrelated probands who have clinical symptoms of PCD and harbor pathogenic variants in *GAS2L2*. Proband PCD-1367 carries an apparent homozygous frameshift variant (c.887_890delTAAG [p. Val296Glyfs*13]), and proband DCP-1040 harbors

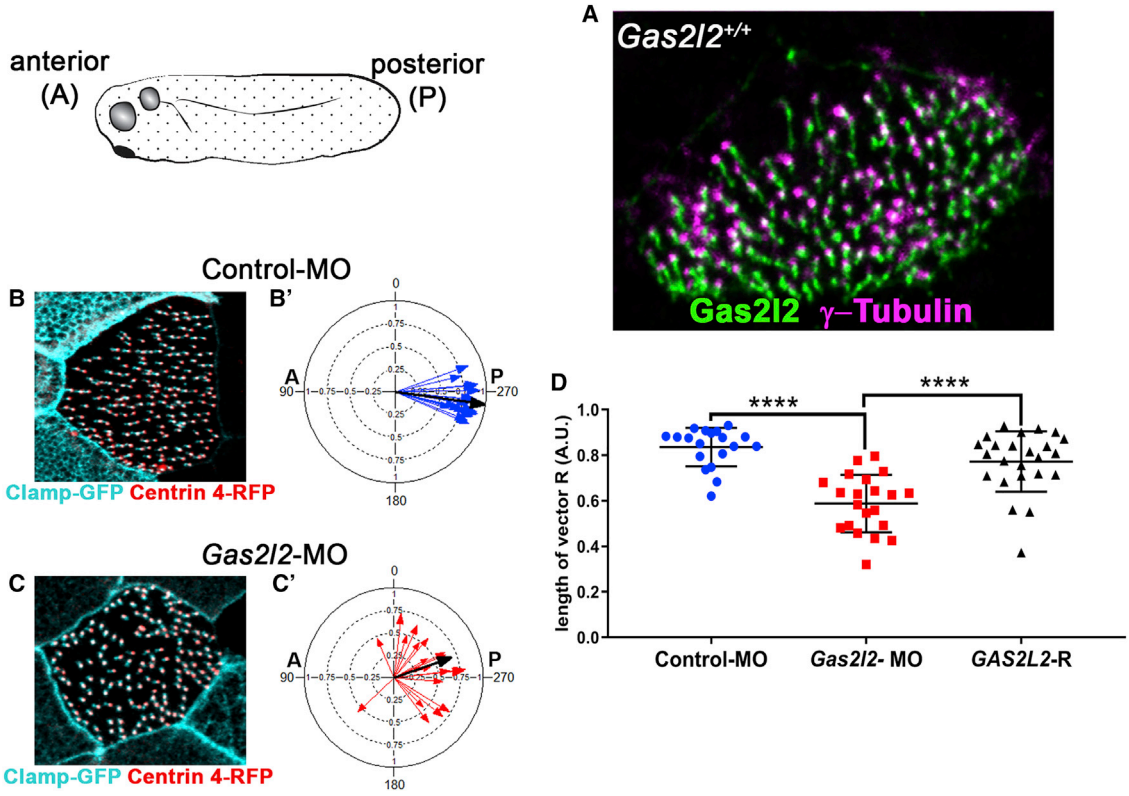

Figure 6. Absence of *Gas2l2* in *X. laevis* Affects Cilia Rotational Polarity
(A) Detection of Gas2l2 in a wild-type skin ciliated cell by immunofluorescence.
(B and C) Representative immunofluorescence images visualizing basal bodies (Clamp-GFP) and rootlet (Centrin 4-RFP) to score basal body-rootlet alignment.
(B′ and C′) Alignment of the basal body and rootlet in control-MO (n = 19, mean vector, black arrow, r = 0.98, CSD = 11.5°) and *Gas2l2*-MO (n = 21, r = 0.67, CSD = 51.2).
(D) The vector length (R) of each analyzed cell is represented in the graph. The average length of the vector was significantly shorter in *Gas2l2*-MO (R = 0.5884 ± 0.1259) cells than in controls (R = 0.836 ± 0.0847). The introduction of human *GAS2L2* mRNA in morpholino-treated embryos (*GAS2L2-R*) rescued the phenotype (n = 23, R = 0.7728 ± 0.1322) (ANOVA, multiple comparison, $p < 0.0001$).

compound heterozygous variants (c.887_890delTAAG [p.Val296Glyfs*13] and c.867_*343+1207del p.?), consistent with a likely recessive trait. Interestingly, more than 400 unrelated individuals with symptoms of PCD were screened, but none harbored bi-allelic variants in *GAS2L2*. The pathogenic variants that we describe are rare in the public databases. For example, in gnomAD[65] the c.887_890delTAAG variant had an allele frequency of 4.924×10^{-4} (130 of 276,682 alleles); none were homozygous. Thus, on the basis of allele frequency, the chance that this variant would appear in a homozygous state is approximately one in 4.5 million individuals. The *GAS2L2* genetic variants were considered pathogenic because (1) *GAS2L2* showed coordinated expression with multiple other genes known to be associated with human PCD in UGET,[66] (2) both variants are predicted to produce a truncated protein or no protein, and (3) *GAS2L2* is not implicated in any other inherited disorder.

Both affected individuals had normal ciliary axonemal ultrastructure by TEM. Several studies have provided examples of individuals who suffer from PCD but have normal ultrastructure of the ciliary axoneme by TEM; for example, such individuals might have genetic variants in *DNAH11*[67] [MIM: 603339] or *CCDC65*[68] [MIM: 611088]. Although in these cases the ciliary axoneme appears normal, the variants result in a stiff and hyperkinetic ciliary beat.[67,68] In contrast, *GAS2L2*-deficient ciliated cells had a normal waveform but a hyperkinetic ciliary beat. Importantly, the orientation of basal bodies, and therefore the direction of ciliary beating, was disrupted. Previously, the disorientation of cilia was described in several cases of PCD.[69–71] In all these cases, the cilia had normal axonemal ultrastructure and a normal ciliary beat frequency, but they had impaired ciliary orientation and clearance. Because of these reports, it was suggested that ciliary disorientation could be a different variant of PCD. However, ciliary disorientation was also found in individuals with chronic respiratory-tract inflammation, and it was reversed by treatment with antibiotics.[72] This suggested that ciliary disorientation was a secondary effect of infection or inflammation and was not the cause of PCD. Independent of the causes leading to disorientation of the cilia, these

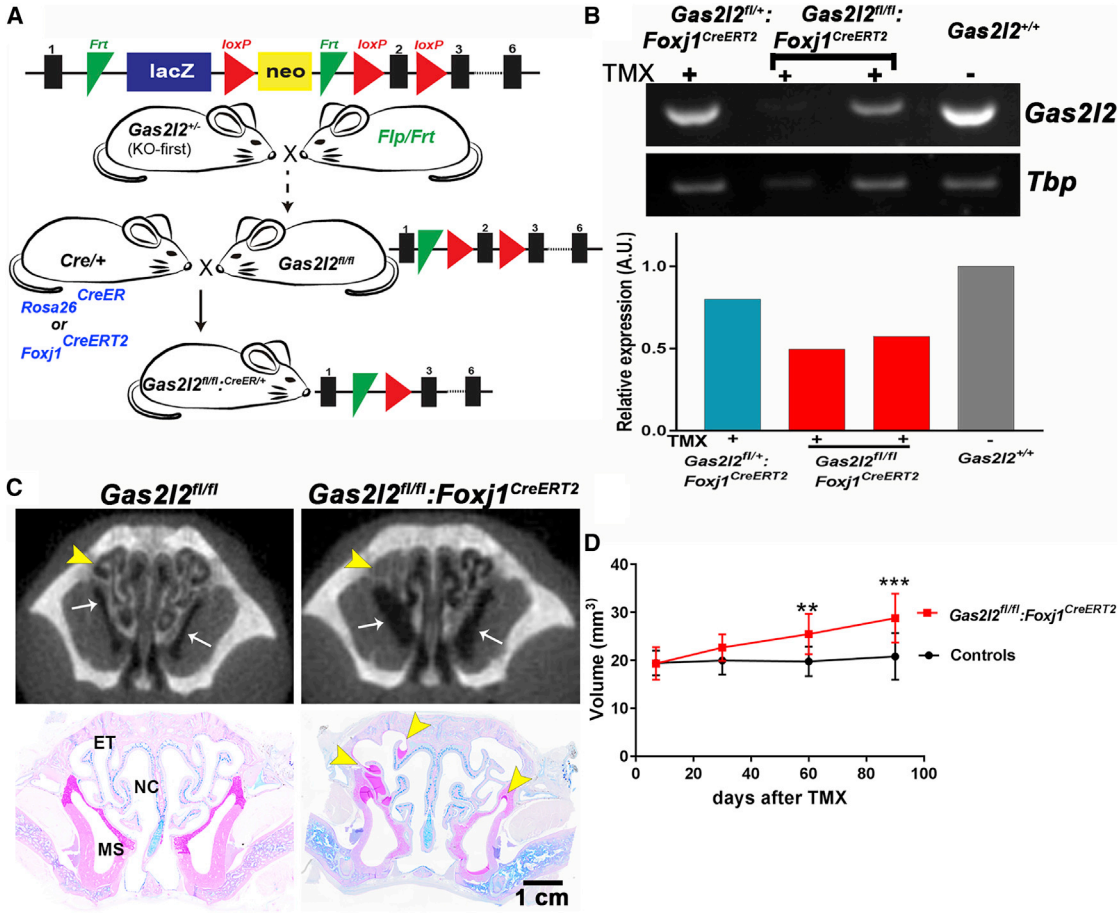

Figure 7. Partial Deletion of *Gas2l2* in Mice Induces a PCD-like Phenotype

(A) Schematic representation of the generation of *Gas2l2*-conditional-KO mouse. See Material and Methods for details.

(B) Reduced expression of *Gas2l2* was confirmed by RT-PCR with RNA extracted from trachea rings. *Tbp* was used as reference for normalization.

(C) Representative micro-CT scan and AB-PAS histology of animal heads after 90 days of treatment. Mucus accumulation in the turbinate (arrow head) and increased volume of the sinuses (arrow) was observed in the conditional-KO mice but not in the control. Abbreviations are as follows: ET, ethmoturbinates; MS, maxillary sinus; and NC, nasal cavity.

(D) Measurement of total nasal-cavity air space in all the animals (n = 41) included in these experiments. A significant increase in nasal air space in the conditional-KO mice (red line) compared to controls (black line) was first observed at 60 days after treatment (each data point corresponds to the mean + SD; **p = 0.0013; ***p = 0.0003, Student's t test, Welch-corrected).

previous results showed that, although the subjects had normal ciliary structure and waveform, MCC was inefficient. More recently, variants in *RPGR* [MIM: 300029] have been shown to cause an X-linked PCD variant associated with ciliary disorientation,[73] and a genetic variant in *STK36* [MIM: 605030] caused disorientation of cilia in an individual with PCD.[4] Here we show that ciliary disorientation can occur as a direct result of a genetic lesion in *GAS2L2,* and the PCD phenotype observed is due to inefficient MCC that results from improper ciliary orientation.

The proband carrying the apparent homozygous variant in *GAS2L2* (PCD-1367) has a rate of nNO production within the normal range.[63] In contrast, the proband carrying the compound heterozygous variant in *GAS2L2* (DCP-1040) has a low rate of nNO production.[74] The difference between nNO values could be due to the age of the subjects, their overall health status at the time of measurement, and/or other genetic or environmental factors. In healthy individuals, NO is produced constitutively within the paranasal sinuses and in the nasal mucosa in response to inflammation,[75] but individuals with chronic rhinosinusitis have a decreased rate of nNO production.[76] The biological significance of NO in the nasal region remains unclear, but it might be essential for local host defense[77] and the regulation of MCC in the respiratory tract.[78] The mechanisms involved in the reduced production of nNO found in most PCD subjects are unknown; more studies will need to clarify the role of ciliary function in the production of nNO.

Until this study, no evidence of the localization, expression, or role of *GAS2L2* in airway cells was available. Here we show that the expression of *GAS2L2* follows a similar pattern to that of other cilia-specific genes.[79] Although we were able to immunoprecipitate GAS2L2 from cultured

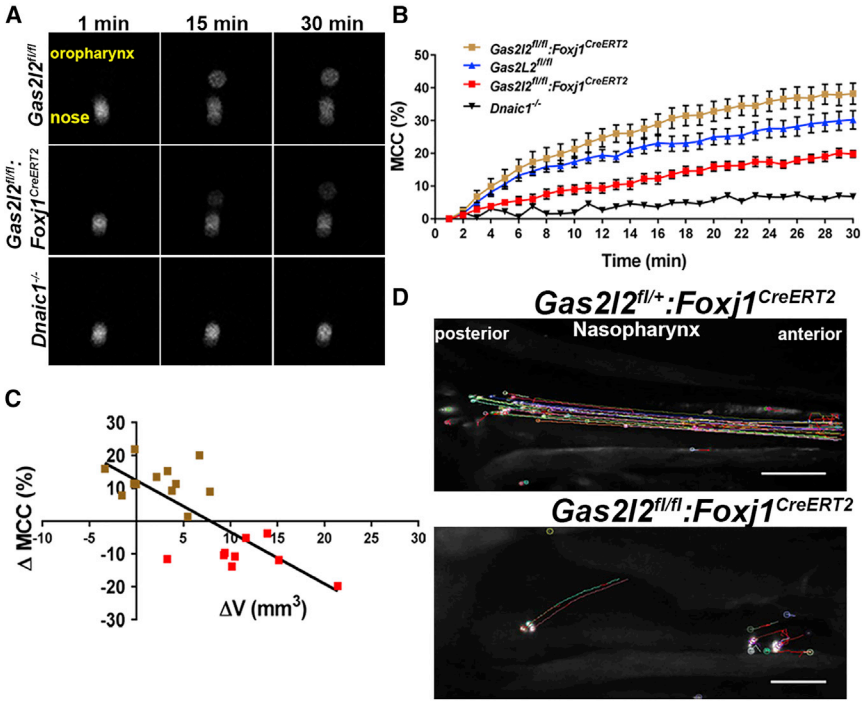

Figure 8. Deletion of *Gas2l2* Affects Mucociliary Clearance in Mice

(A) Representative scintigraphy images of real-time measurements of nasal clearance in mice via Technetium-99. Radiolabeled particles were delivered into the nose (left panel). The clearance was recorded over time (middle and right panels) with a gamma camera.

(B) Cumulative nasal clearance in *Gas2l2*-conditional-KO (n = 21), controls (n = 20), and *Dnaic1*$^{-/-}$ (n = 3) treated with TMX. In the *Gas2l2*-conditional-KO two groups were observed: a group with normal clearance (brown squares, n = 12) and a group with impaired clearance (red squares, n = 9).

(C) Correlation between the change in MCC in *Gas2l2*-conditional-KO mice relative to controls and ΔV in the two groups of *Gas2l2*-conditional-KO mice ($r = -0.7151$, $p = 0.0018$).

(D) Time-lapse images of 600 frames (5 frames/s) representing the nasopharyngeal clearance of fluorescence beads in control and *Gas2l2*-conditional-KO mice (the scale bar represents 0.5 mm).

airway cells, co-immunoprecipitation studies aimed at identifying interacting proteins were unsuccessful (not shown). However, using a combination of high-resolution SIM and single-molecule GSD microscopy, we detected GAS2L2 localizing closely with markers of basal bodies (γ-tubulin and centrin-2) and basal feet (centriolin), and in the proximity of actin filaments and the rootlet. These results, together with the known ability of GAS2L2 to bind both actin and microtubules,[25] suggest that in ciliated cells GAS2L2 is part of the protein network at the base of the ciliary axoneme and could provide mechanical support to the cilia during the constant physical stress of ciliary beating. GAS2L2 could mediate the crosstalk between microtubules, actin filaments, and the proteins that constitute the basal body and its appendages, thus ensuring the proper orientation/stabilization of basal bodies and coordination of the ciliary beating. In *GAS2L2*-deficient human cells the basal bodies were significantly less aligned than control cells. This phenotype was recapitulated in *Gas2l2*$^{-/-}$ mTEC and in *X. laevis* embryos injected with antisense *Gas2l2*-MO. These results suggest a conserved role for GAS2L2 in the alignment of basal bodies. Previous studies in *X. laevis* and mice showed that the docking of basal bodies at the membrane and their relative spacing at the apical cortex is driven by the actin cytoskeleton,[15] whereas cortical microtubules are important for the alignment of basal bodies.[15,80] In human and mTEC *GAS2L2*-deficient cells, the basal bodies were normally spaced, but their alignment was impaired. This suggests that the lack of GAS2L2 does not disrupt the actin cytoskeleton but might affect the stabilization of cortical MT and, subsequently, basal body alignment. It will be interesting to look in detail and over time at the organization of the microtubule network at the base of the cilium in *GAS2L2*-deficient cells. In contrast, in *X. laevis* embryos injected with antisense *Gas2l2*-MO targeting both Gas2l2 isoforms, we observed a decrease in both the number and alignment of basal bodies. The severity of the phenotype suggests that the Gas2l2 isoforms play other roles independent of their role in cilia orientation.

Surprisingly, *Gas2l2*-knockout mice die neonatally. The high lethality in *Gas2l2*$^{-/-}$ mice could be associated with developmental defects. During early embryogenesis, the motile cilia at the embryonic node generates the right-to-left flow required for establishing the left-right body axis,[81] resulting in the normal localization of the organs in the body (situs solitus). We observed situs defects in 50% (3/6) of the *Gas2l2*$^{-/-}$ mouse embryos dissected at 18.5 dpc, suggesting that GAS2L2 might be necessary for proper ciliary function at the embryonic node. Another common phenotype in mouse models of PCD is hydrocephalus.[82] Hydrocephalic PCD mice develop enlarged heads as a result of ventricular dilatation during the neonatal period and die within the first month of life.[82,83] Although we observed hydrocephalus in the two *Gas2l2*$^{-/-}$ mice that survived, it is unlikely to be the primary cause of neonatal death in the *Gas2l2*$^{-/-}$ mice. The development of hydrocephalus could be related to other genetic modifiers that play a role in the susceptibility to severe PCD-associated hydrocephalus in the C57BL/6J background.[82,84] Additionally, the majority of the GAS2 family members have been implicated in controlling cell proliferation and apoptosis. For example, GAS2 is required for proper follicular development in mice,[31] GAS2L1 might be important for the maintenance of genome stability by controlling centriole motility and ensuring the timing

of centrosome disjunction during cell division,[32] and GAS2L3 is important for brain morphogenesis and development.[36] The fact that human and mouse *GAS2L2*-deficient airway cells proliferate and differentiate normally in culture suggests that GAS2L2 might not play a role in regulating cell proliferation or differentiation. However, in the *Gas2l2*$^{-/-}$ mice, GAS2L2 might be important for maintaining homeostasis in the tissues in which it is expressed. These phenotypes of the *Gas2l2*$^{-/-}$ mice—neonatal death, situs abnormalities, and hydrocephalus—require further investigation.

The conditional deletion of *Gas2l2 in vivo* caused the typical mouse PCD phenotype: impaired MCC accompanied by mucus accumulation in the nasal cavity and remodeling of the nasal cavity. In *Gas2l2*-conditional-KO mice we observed significantly impaired clearance directionality in the nasopharynx and a significant correlation between impaired MCC and nasal remodeling. We observed that ~20% of the conditional-KO mice included in the study had normal MCC, no change in nasal air space, and no mucus accumulation, most likely because the tamoxifen treatment was insufficient to completely delete *Gas2l2*. This possibility is supported by data showing expression of *Gas2l2* in tamoxifen-treated mice. Alternatively, in the unaffected mice the deletion of *Gas2l2* could require more time to show its effect. The tamoxifen treatment started when the mice were 4 weeks old; thus, the animals possessed a full complement of properly orientated cilia. Although previous studies have suggested that ciliated cells and ciliary proteins are very stable,[64,85] the turnover of ciliated cells and ciliary proteins *in vivo* is unknown. Our results suggest that over time all mice lacking *Gas2l2* will develop PCD.

In summary, we propose that GAS2L2 plays a critical role in the airways by inter-connecting cytoskeletal elements, basal bodies, and basal feet. Thus, GAS2L2 helps to maintain the correct orientation of basal bodies in ciliated cells. Our results demonstrate that the proper orientation of the cilia is crucial for ensuring effective MCC and that pathogenic variants in *GAS2L2* result in poorly aligned cilia, a hyperkinetic ciliary beat, and PCD.

Accession Numbers

c.867_*343+1207del p.? has been deposited in LOVD: 0000439768.

Supplemental Data

The Supplemental Data include Supplemental Material and Methods, nine figures, six tables, and six videos and can be found with this article online at https://doi.org/10.1016/j.ajhg.2018.12.009.

Acknowledgments

The authors would like to thank the PCD subjects and family members for their participation and thank the US PCD Foundation and the investigators and coordinators of the Genetic Disorders of Mucociliary Clearance Consortium, part of the Rare Disease Clinical Research Network. We thank Jay Shendure, Deborah Nickerson, and Michael Bamshad from University of Washington School of Medicine (National Institutes of Health [NHI]/ National Human Genome Research Institute [NHGRI] U54HG0006493), Seattle GO Sequencing Project (HL-102926), RS & G at Northwest Genomics Center at the University of Washington (NIH-National Heart, Lung, and Blood Institute [NHLBI] HHSN268201100037); Shrikant Mane, Francesc Lopez-Giraldez, and Weilai Dong from the Yale Center (UM1 HG006504) for whole-exome sequencing and bioinformatics support; Kimberly Burns for histology and electron-microscopy support; Whitney Wolf and Lu Huang for technical assistance; Hong Dang for bioinformatics assistance; Robert Tarran for providing the Leica Sp8 confocal and GSD microscopes; Michael Chua and Tony Perdue for assistance with confocal imaging; Frank Conlon and Panna Tandon for providing *Xenopus laevis* oocytes; Uma Nagarajan and Amy Kiatthanapaiboon for providing samples of human fallopian-tube total RNA; Julie Kimbell for assistance with Mimics Research 18.0; and Scott H. Randell and the UNC Cell Culture Core for providing human airway cells. The UNC Cell Core Facility is supported by BOUCHE15R0 and P30DK065988 grants. The UNC Proteomics Core Facility is supported in part by P30 CA016086. The Small Animal Imaging Facility at the UNC Biomedical Imaging Research Center is supported in part by a National Cancer Institute cancer core grant, P30-CA016086-40. Funding support for this research was provided to B.J.M. by R01GM089970 from the National Institute of General Medical Sciences at the NIH; to M.R.K and M.A.Z by grant 5U54HL096458 from the Office of Rare Diseases Research and NHLBI at the NIH ; to M.R.K., L.E.O., and M.A.Z. by NIH-NHLBI grant R01HL071798; to L.E.O., M.A.Z., and M.R.K by NIH-NHLBI grant R01HL117836; and to the University of North Carolina at Chapel Hill by grant UL1 TR000083 from the National Center for Advancing Translational Sciences at the NIH. Work by S.A., E.E., M.L., and L.T. is supported by the Fondation pour la Recherche Médicale grant DEQ20120323689, by Institut National de la Santé et de la Recherche Médicale (INSERM) grant ANR-10-COHO-003, and the Legs Poix grant from the Chancellerie des Universités of Sorbonne Université.

Declaration of Interests

The authors declare no competing interests.

Received: August 20, 2018
Accepted: December 14, 2018
Published: January 17, 2019

Web Resources

1000 Genomes, http://www.internationalgenome.org/
dbSNP, https://www.ncbi.nlm.nih.gov/snp
Ensembl, http://grch37.ensembl.org/Homo_sapiens/Info/Index
GenBank, https://www.ncbi.nlm.nih.gov/genbank/
gnomAD, http://gnomad.broadinstitute.org/
IGV, https://software.broadinstitute.org/software/igv/
LOVD, https://databases.lovd.nl/shared/variants
NIBB, http://xenopus.nibb.ac.jp/
OMIM, http://www.omim.org/
Uniprot, https://www.uniprot.org/

References

1. Knowles, M.R., Zariwala, M., and Leigh, M. (2016). Primary Ciliary Dyskinesia. Clin. Chest Med. *37*, 449–461.
2. Shapiro, A.J., Zariwala, M.A., Ferkol, T., Davis, S.D., Sagel, S.D., Dell, S.D., Rosenfeld, M., Olivier, K.N., Milla, C., Daniel, S.J., et al. (2016). Diagnosis, monitoring, and treatment of primary ciliary dyskinesia: PCD foundation consensus recommendations based on state of the art review. Pediatr. Pulmonol *51*, 115–132. Published online September 29, 2015.
3. Zariwala, M.A., Knowles, M.R., and Leigh, M.W. (2007 [Updated 2015]). Primary Ciliary Dyskinesia. In GeneReviews, R.A. Pagon, M.P. Adam, H.H. Ardinger, S.E. Wallace, A. Amemiya, L.J.H. Bean, T.D. Bird, N. Ledbetter, H.C. Mefford, and R.J.H. Smith, et al., eds. (University of Washington).
4. Edelbusch, C., Cindrić, S., Dougherty, G.W., Loges, N.T., Olbrich, H., Rivlin, J., Wallmeier, J., Pennekamp, P., Amirav, I., and Omran, H. (2017). Mutation of serine/threonine protein kinase 36 (STK36) causes primary ciliary dyskinesia with a central pair defect. Hum. Mutat. *38*, 964–969.
5. Olcese, C., Patel, M.P., Shoemark, A., Kiviluoto, S., Legendre, M., Williams, H.J., Vaughan, C.K., Hayward, J., Goldenberg, A., Emes, R.D., et al. (2017). X-linked primary ciliary dyskinesia due to mutations in the cytoplasmic axonemal dynein assembly factor PIH1D3. Nat. Commun. *8*, 14279.
6. Paff, T., Loges, N.T., Aprea, I., Wu, K., Bakey, Z., Haarman, E.G., Daniels, J.M.A., Sistermans, E.A., Bogunovic, N., Dougherty, G.W., et al. (2017). Mutations in PIH1D3 cause X-linked primary ciliary dyskinesia with outer and inner dynein arm defects. Am. J. Hum. Genet. *100*, 160–168.
7. Wallmeier, J., Shiratori, H., Dougherty, G.W., Edelbusch, C., Hjeij, R., Loges, N.T., Menchen, T., Olbrich, H., Pennekamp, P., Raidt, J., et al. (2016). TTC25 deficiency results in defects of the outer dynein arm docking machinery and primary ciliary dyskinesia with left-right body asymmetry randomization. Am. J. Hum. Genet. *99*, 460–469.
8. El Khouri, E., Thomas, L., Jeanson, L., Bequignon, E., Vallette, B., Duquesnoy, P., Montantin, G., Copin, B., Dastot-Le Moal, F., Blanchon, S., et al. (2016). Mutations in DNAJB13, encoding an HSP40 family member, cause primary ciliary dyskinesia and male infertility. Am. J. Hum. Genet. *99*, 489–500.
9. Höben, I.M., Hjeij, R., Olbrich, H., Dougherty, G.W., Nöthe-Menchen, T., Aprea, I., Frank, D., Pennekamp, P., Dworniczak, B., Wallmeier, J., et al. (2018). Mutations in C11orf70 cause primary ciliary dyskinesia with randomization of left/right body asymmetry due to defects of outer and inner dynein arms. Am. J. Hum. Genet. *102*, 973–984.
10. Fassad, M.R., Shoemark, A., le Borgne, P., Koll, F., Patel, M., Dixon, M., Hayward, J., Richardson, C., Frost, E., Jenkins, L., et al. (2018). C11orf70 mutations disrupting the intraflagellar transport-dependent assembly of multiple axonemal dyneins cause primary ciliary dyskinesia. Am. J. Hum. Genet. *102*, 956–972.
11. Olbrich, H., Cremers, C., Loges, N.T., Werner, C., Nielsen, K.G., Marthin, J.K., Philipsen, M., Wallmeier, J., Pennekamp, P., Menchen, T., et al. (2015). Loss-of-function GAS8 mutations cause primary ciliary dyskinesia and disrupt the nexin-dynein regulatory complex. Am. J. Hum. Genet. *97*, 546–554.
12. Bonnefoy, S., Watson, C.M., Kernohan, K.D., Lemos, M., Hutchinson, S., Poulter, J.A., Crinnion, L.A., Berry, I., Simmonds, J., Vasudevan, P., et al.; Care4Rare Canada Consortium (2018). Biallelic mutations in LRRC56, encoding a protein associated with intraflagellar transport, cause mucociliary clearance and laterality defects. Am. J. Hum. Genet. *103*, 727–739.
13. Bustamante-Marin, X.M., and Ostrowski, L.E. (2017). Cilia and mucociliary clearance. Cold Spring Harb. Perspect. Biol. *9*, 9.
14. Vladar, E.K., Bayly, R.D., Sangoram, A.M., Scott, M.P., and Axelrod, J.D. (2012). Microtubules enable the planar cell polarity of airway cilia. Curr. Biol. *22*, 2203–2212.
15. Werner, M.E., Hwang, P., Huisman, F., Taborek, P., Yu, C.C., and Mitchell, B.J. (2011). Actin and microtubules drive differential aspects of planar cell polarity in multiciliated cells. J. Cell Biol. *195*, 19–26.
16. Marshall, W.F. (2008). Basal Bodies: Platforms for Building Cilia. In Current Topics in Developmental Biology Wassarman, M. Paul, ed. (Academic Press), pp. 1–22.
17. Vertii, A., Hung, H.-F., Hehnly, H., and Doxsey, S. (2016). Human basal body basics. Cilia *5*, 13.
18. Yang, J., Gao, J., Adamian, M., Wen, X.H., Pawlyk, B., Zhang, L., Sanderson, M.J., Zuo, J., Makino, C.L., and Li, T. (2005). The ciliary rootlet maintains long-term stability of sensory cilia. Mol. Cell. Biol. *25*, 4129–4137.
19. Kunimoto, K., Yamazaki, Y., Nishida, T., Shinohara, K., Ishikawa, H., Hasegawa, T., Okanoue, T., Hamada, H., Noda, T., Tamura, A., et al. (2012). Coordinated ciliary beating requires Odf2-mediated polarization of basal bodies via basal feet. Cell *148*, 189–200.
20. Raidt, J., Wallmeier, J., Hjeij, R., Onnebrink, J.G., Pennekamp, P., Loges, N.T., Olbrich, H., Häffner, K., Dougherty, G.W., Omran, H., and Werner, C. (2014). Ciliary beat pattern and frequency in genetic variants of primary ciliary dyskinesia. Eur. Respir. J. *44*, 1579–1588.
21. Chilvers, M.A., Rutman, A., and O'Callaghan, C. (2003). Ciliary beat pattern is associated with specific ultrastructural defects in primary ciliary dyskinesia. J. Allergy Clin. Immunol. *112*, 518–524.
22. Baum, G.L., Zwas, S.T., Katz, I., and Roth, Y. (1990). Mucociliary clearance from central airways in patients with excessive sputum production with and without primary ciliary dyskinesia. Chest *98*, 608–612.
23. Noone, P.G., Bennett, W.D., Regnis, J.A., Zeman, K.L., Carson, J.L., King, M., Boucher, R.C., and Knowles, M.R. (1999). Effect of aerosolized uridine-5′-triphosphate on airway clearance with cough in patients with primary ciliary dyskinesia. Am. J. Respir. Crit. Care Med. *160*, 144–149.
24. Goriounov, D., Leung, C.L., and Liem, R.K. (2003). Protein products of human Gas2-related genes on chromosomes 17 and 22 (hGAR17 and hGAR22) associate with both microfilaments and microtubules. J. Cell Sci. *116*, 1045–1058.
25. Stroud, M.J., Nazgiewicz, A., McKenzie, E.A., Wang, Y., Kammerer, R.A., and Ballestrem, C. (2014). GAS2-like proteins mediate communication between microtubules and actin through interactions with end-binding proteins. J. Cell Sci. *127*, 2672–2682.
26. Jiang, K., Toedt, G., Montenegro Gouveia, S., Davey, N.E., Hua, S., van der Vaart, B., Grigoriev, I., Larsen, J., Pedersen, L.B., Bezstarosti, K., et al. (2012). A Proteome-wide screen for mammalian SxIP motif-containing microtubule plus-end tracking proteins. Curr. Biol. *22*, 1800–1807.
27. Collavin, L., Buzzai, M., Saccone, S., Bernard, L., Federico, C., DellaValle, G., Brancolini, C., and Schneider, C. (1998). cDNA characterization and chromosome mapping of the human GAS2 gene. Genomics *48*, 265–269.

28. Brancolini, C., Benedetti, M., and Schneider, C. (1995). Microfilament reorganization during apoptosis: the role of Gas2, a possible substrate for ICE-like proteases. EMBO J. *14*, 5179–5190.
29. Zhang, T., Dayanandan, B., Rouiller, I., Lawrence, E.J., and Mandato, C.A. (2011). Growth-arrest-specific protein 2 inhibits cell division in Xenopus embryos. PLoS ONE *6*, e24698.
30. Zhou, H., Ge, Y., Sun, L., Ma, W., Wu, J., Zhang, X., Hu, X., Eaves, C.J., Wu, D., and Zhao, Y. (2014). Growth arrest specific 2 is up-regulated in chronic myeloid leukemia cells and required for their growth. PLoS ONE *9*, e86195.
31. York, J.P., Ren, Y.A., Zeng, J., Bin Zhang, Wang, F., Chen, R., Liu, J., Xia, X., and Zhang, P. (2016). Growth arrest specific 2 (GAS2) is a critical mediator of germ cell cyst breakdown and folliculogenesis in mice. Sci. Rep. *6*, 34956.
32. Au, F.K.C., Jia, Y., Jiang, K., Grigoriev, I., Hau, B.K.T., Shen, Y., Du, S., Akhmanova, A., and Qi, R.Z. (2017). GAS2L1 is a centriole-associated protein required for centrosome dynamics and disjunction. Dev. Cell *40*, 81–94.
33. Gamper, I., Koh, K.R., Ruau, D., Ullrich, K., Bartunkova, J., Piroth, D., Hacker, C., Bartunek, P., and Zenke, M. (2009). GAR22: A novel target gene of thyroid hormone receptor causes growth inhibition in human erythroid cells. Exp. Hematol *37*, 539–548.e4.
34. Desmond, J.C., Raynaud, S., Tung, E., Hofmann, W.K., Haferlach, T., and Koeffler, H.P. (2007). Discovery of epigenetically silenced genes in acute myeloid leukemias. Leukemia *21*, 1026–1034.
35. Stroud, M.J., Kammerer, R.A., and Ballestrem, C. (2011). Characterization of G2L3 (GAS2-like 3), a new microtubule- and actin-binding protein related to spectraplakins. J. Biol. Chem. *286*, 24987–24995.
36. Sharaby, Y., Lahmi, R., Amar, O., Elbaz, I., Lerer-Goldshtein, T., Weiss, A.M., Appelbaum, L., and Tzur, A. (2014). Gas2l3 is essential for brain morphogenesis and development. Dev. Biol. *394*, 305–313.
37. Wolter, P., Schmitt, K., Fackler, M., Kremling, H., Probst, L., Hauser, S., Gruss, O.J., and Gaubatz, S. (2012). GAS2L3, a target gene of the DREAM complex, is required for proper cytokinesis and genomic stability. J. Cell Sci. *125*, 2393–2406.
38. Wu, Y.-C., Lai, H.-L., Chang, W.-C., Lin, J.-T., Liu, Y.-J., and Chern, Y. (2013). A novel Gαs-binding protein, Gas-2 like 2, facilitates the signaling of the A2A adenosine receptor. Biochim. Biophys. Acta *1833*, 3145–3154.
39. Knowles, M.R., Ostrowski, L.E., Leigh, M.W., Sears, P.R., Davis, S.D., Wolf, W.E., Hazucha, M.J., Carson, J.L., Olivier, K.N., Sagel, S.D., et al. (2014). Mutations in RSPH1 cause primary ciliary dyskinesia with a unique clinical and ciliary phenotype. Am. J. Respir. Crit. Care Med. *189*, 707–717.
40. Fulcher, M.L., and Randell, S.H. (2013). Human nasal and tracheo-bronchial respiratory epithelial cell culture. Methods Mol. Biol. *945*, 109–121.
41. Müller, L., Brighton, L.E., Carson, J.L., Fischer, W.A., 2nd, and Jaspers, I. (2013). Culturing of human nasal epithelial cells at the air liquid interface. J. Vis. Exp. (80).
42. Gentzsch, M., Boyles, S.E., Cheluvaraju, C., Chaudhry, I.G., Quinney, N.L., Cho, C., Dang, H., Liu, X., Schlegel, R., and Randell, S.H. (2017). Pharmacological rescue of conditionally reprogrammed cystic fibrosis bronchial epithelial cells. Am. J. Respir. Cell Mol. Biol. *56*, 568–574.
43. You, Y., Richer, E.J., Huang, T., and Brody, S.L. (2002). Growth and differentiation of mouse tracheal epithelial cells: selection of a proliferative population. Am. J. Physiol. Lung Cell. Mol. Physiol. *283*, L1315–L1321.
44. He, J.Q., Sandford, A.J., Wang, I.M., Stepaniants, S., Knight, D.A., Kicic, A., Stick, S.M., and Paré, P.D. (2008). Selection of housekeeping genes for real-time PCR in atopic human bronchial epithelial cells. Eur. Respir. J. *32*, 755–762.
45. Yüzbaşioğlu, A., Onbaşilar, I., Kocaefe, C., and Ozgüç, M. (2010). Assessment of housekeeping genes for use in normalization of real time PCR in skeletal muscle with chronic degenerative changes. Exp. Mol. Pathol. *88*, 326–329.
46. Blackburn, K., Bustamante-Marin, X., Yin, W., Goshe, M.B., and Ostrowski, L.E. (2017). Quantitative proteomic analysis of human airway cilia identifies previously uncharacterized proteins of high abundance. J. Proteome Res. *16*, 1579–1592.
47. Schindelin, J., Arganda-Carreras, I., Frise, E., Kaynig, V., Longair, M., Pietzsch, T., Preibisch, S., Rueden, C., Saalfeld, S., Schmid, B., et al. (2012). Fiji: An open-source platform for biological-image analysis. Nat. Methods *9*, 676–682.
48. Dunn, K.W., Kamocka, M.M., and McDonald, J.H. (2011). A practical guide to evaluating colocalization in biological microscopy. Am. J. Physiol. Cell Physiol. *300*, C723–C742.
49. Schneider, C.A., Rasband, W.S., and Eliceiri, K.W. (2012). NIH Image to ImageJ: 25 years of image analysis. Nat. Methods *9*, 671–675.
50. Sears, P.R., Yin, W.N., and Ostrowski, L.E. (2015). Continuous mucociliary transport by primary human airway epithelial cells in vitro. Am. J. Physiol. Lung Cell. Mol. Physiol. *309*, L99–L108.
51. Reynolds, E.S. (1963). The use of lead citrate at high pH as an electron-opaque stain in electron microscopy. J. Cell Biol. *17*, 208–212.
52. Batschelet, E. (1981). Circular Statistics in Biology. In Mathematics in Biology, R. Sibson and C.J.E., eds. (Academic Press), p. 371.
53. Skarnes, W.C., Rosen, B., West, A.P., Koutsourakis, M., Bushell, W., Iyer, V., Mujica, A.O., Thomas, M., Harrow, J., Cox, T., et al. (2011). A conditional knockout resource for the genome-wide study of mouse gene function. Nature *474*, 337–342.
54. Muthusamy, N., Vijayakumar, A., Cheng, G., and Ghashghaei, H.T. (2014). A knock-in Foxj1(CreERT2:GFP) mouse for recombination in epithelial cells with motile cilia. Genesis *52*, 350–358.
55. Hayashi, S., and McMahon, A.P. (2002). Efficient recombination in diverse tissues by a tamoxifen-inducible form of Cre: a tool for temporally regulated gene activation/inactivation in the mouse. Dev. Biol. *244*, 305–318.
56. Hua, X., Zeman, K.L., Zhou, B., Hua, Q., Senior, B.A., Tilley, S.L., and Bennett, W.D. (2010). Noninvasive real-time measurement of nasal mucociliary clearance in mice by pinhole gamma scintigraphy. J. Appl. Physiol. *108*, 189–196.
57. Grubb, B.R., Livraghi-Butrico, A., Rogers, T.D., Yin, W., Button, B., and Ostrowski, L.E. (2016). Reduced mucociliary clearance in old mice is associated with a decrease in Muc5b mucin. Am. J. Physiol. Lung Cell. Mol. Physiol. *310*, L860–L867.
58. Xiao, X., Geyer, V.F., Bowne-Anderson, H., Howard, J., and Sbalzarini, I.F. (2016). Automatic optimal filament segmentation with sub-pixel accuracy using generalized linear models and B-spline level-sets. Med. Image Anal. *32*, 157–172.
59. Ostrowski, L.E., Yin, W., Rogers, T.D., Busalacchi, K.B., Chua, M., O'Neal, W.K., and Grubb, B.R. (2010). Conditional deletion of dnaic1 in a murine model of primary ciliary dyskinesia

causes chronic rhinosinusitis. Am. J. Respir. Cell Mol. Biol. *43*, 55–63.
60. Sive, H.L., Grainger, R.M., and Harland, R.M. (2000). Early development of Xenopus laevis: A laboratory manual (Cold Spring Harbor Laboratory Press).
61. Werner, M.E., and Mitchell, B.J. (2013). Using Xenopus skin to study cilia development and function. Methods Enzymol. *525*, 191–217.
62. Mitchell, B., Jacobs, R., Li, J., Chien, S., and Kintner, C. (2007). A positive feedback mechanism governs the polarity and motion of motile cilia. Nature *447*, 97–101.
63. Leigh, M.W., Hazucha, M.J., Chawla, K.K., Baker, B.R., Shapiro, A.J., Brown, D.E., Lavange, L.M., Horton, B.J., Qaqish, B., Carson, J.L., et al. (2013). Standardizing nasal nitric oxide measurement as a test for primary ciliary dyskinesia. Ann. Am. Thorac. Soc. *10*, 574–581.
64. Ostrowski, L.E., Yin, W., Patel, M., Sechelski, J., Rogers, T., Burns, K., Grubb, B.R., and Olsen, J.C. (2014). Restoring ciliary function to differentiated primary ciliary dyskinesia cells with a lentiviral vector. Gene Ther. *21*, 253–261.
65. Lek, M., Karczewski, K.J., Minikel, E.V., Samocha, K.E., Banks, E., Fennell, T., O'Donnell-Luria, A.H., Ware, J.S., Hill, A.J., Cummings, B.B., et al.; Exome Aggregation Consortium (2016). Analysis of protein-coding genetic variation in 60,706 humans. Nature *536*, 285–291.
66. Day, A., Dong, J., Funari, V.A., Harry, B., Strom, S.P., Cohn, D.H., and Nelson, S.F. (2009). Disease gene characterization through large-scale co-expression analysis. PLoS ONE *4*, e8491.
67. Schwabe, G.C., Hoffmann, K., Loges, N.T., Birker, D., Rossier, C., de Santi, M.M., Olbrich, H., Fliegauf, M., Failly, M., Liebers, U., et al. (2008). Primary ciliary dyskinesia associated with normal axoneme ultrastructure is caused by DNAH11 mutations. Hum. Mutat. *29*, 289–298.
68. Horani, A., Brody, S.L., Ferkol, T.W., Shoseyov, D., Wasserman, M.G., Ta-shma, A., Wilson, K.S., Bayly, P.V., Amirav, I., Cohen-Cymberknoh, M., et al. (2013). CCDC65 mutation causes primary ciliary dyskinesia with normal ultrastructure and hyperkinetic cilia. PLoS ONE *8*, e72299.
69. Rutland, J., and de Iongh, R.U. (1990). Random ciliary orientation. A cause of respiratory tract disease. N. Engl. J. Med. *323*, 1681–1684.
70. Rutman, A., Cullinan, P., Woodhead, M., Cole, P.J., and Wilson, R. (1993). Ciliary disorientation: a possible variant of primary ciliary dyskinesia. Thorax *48*, 770–771.
71. Rayner, C.F., Rutman, A., Dewar, A., Greenstone, M.A., Cole, P.J., and Wilson, R. (1996). Ciliary disorientation alone as a cause of primary ciliary dyskinesia syndrome. Am. J. Respir. Crit. Care Med. *153*, 1123–1129.
72. Rayner, C.F., Rutman, A., Dewar, A., Cole, P.J., and Wilson, R. (1995). Ciliary disorientation in patients with chronic upper respiratory tract inflammation. Am. J. Respir. Crit. Care Med. *151*, 800–804.
73. Bukowy-Bieryłło, Z., Ziętkiewicz, E., Loges, N.T., Wittmer, M., Geremek, M., Olbrich, H., Fliegauf, M., Voelkel, K., Rutkiewicz, E., Rutland, J., et al. (2013). RPGR mutations might cause reduced orientation of respiratory cilia. Pediatr. Pulmonol. *48*, 352–363.
74. Beydon, N., Chambellan, A., Alberti, C., de Blic, J., Clément, A., Escudier, E., and Le Bourgeois, M. (2015). Technical and practical issues for tidal breathing measurements of nasal nitric oxide in children. Pediatr. Pulmonol. *50*, 1374–1382.
75. Lundberg, J.O. (2008). Nitric oxide and the paranasal sinuses. Anat. Rec. (Hoboken) *291*, 1479–1484.
76. Dabholkar, Y.G., Saberwal, A.A., Velankar, H.K., Shetty, A.K., Chordia, N.P., and Budhwani, S.R. (2014). Correlation of nasal nitric oxide measurement with computed tomography findings in chronic rhinosinusitis. Indian J. Otolaryngol. Head Neck Surg. *66*, 92–96.
77. Moncada, S., Palmer, R.M., and Higgs, E.A. (1991). Nitric oxide: physiology, pathophysiology, and pharmacology. Pharmacol. Rev. *43*, 109–142.
78. Runer, T., and Lindberg, S. (1998). Effects of nitric oxide on blood flow and mucociliary activity in the human nose. Ann. Otol. Rhinol. Laryngol. *107*, 40–46.
79. Knowles, M.R., Ostrowski, L.E., Loges, N.T., Hurd, T., Leigh, M.W., Huang, L., Wolf, W.E., Carson, J.L., Hazucha, M.J., Yin, W., et al. (2013). Mutations in SPAG1 cause primary ciliary dyskinesia associated with defective outer and inner dynein arms. Am. J. Hum. Genet. *93*, 711–720.
80. Clare, D.K., Magescas, J., Piolot, T., Dumoux, M., Vesque, C., Pichard, E., Dang, T., Duvauchelle, B., Poirier, F., and Delacour, D. (2014). Basal foot MTOC organizes pillar MTs required for coordination of beating cilia. Nat. Commun. *5*, 4888.
81. Nonaka, S., Tanaka, Y., Okada, Y., Takeda, S., Harada, A., Kanai, Y., Kido, M., and Hirokawa, N. (1998). Randomization of left-right asymmetry due to loss of nodal cilia generating leftward flow of extraembryonic fluid in mice lacking KIF3B motor protein. Cell *95*, 829–837.
82. Lee, L. (2013). Riding the wave of ependymal cilia: genetic susceptibility to hydrocephalus in primary ciliary dyskinesia. J. Neurosci. Res. *91*, 1117–1132.
83. Ibañez-Tallon, I., Gorokhova, S., and Heintz, N. (2002). Loss of function of axonemal dynein Mdnah5 causes primary ciliary dyskinesia and hydrocephalus. Hum. Mol. Genet. *11*, 715–721.
84. Finn, R., Evans, C.C., and Lee, L. (2014). Strain-dependent brain defects in mouse models of primary ciliary dyskinesia with mutations in Pcdp1 and Spef2. Neuroscience *277*, 552–567.
85. Leigh, M.W., Carson, J.L., Gambling, T.M., and Boat, T.F. (1992). Loss of cilia and altered phenotypic expression of ciliated cells after acute sulfur dioxide exposure. Chest *101* (3, Suppl), 16S.